

ATAT 1.01, an Automated Timing Accordance Tool for comparing ice-sheet model output with geochronological data

Jeremy C. Ely¹, Chris D. Clark¹, David Small² and Richard C.A. Hindmarsh³

¹Department of Geography, The University of Sheffield, Sheffield, S10 2TN, UK

²Department of Geography, Durham University, Durham, DH1 3LE, UK

³British Antarctic Survey, High Cross, Madingley Road, Cambridge, CB3 0ET, UK

Correspondence to: Jeremy C. Ely (j.ely@sheffield.ac.uk)

Abstract. Earth's extant ice sheets are of great societal importance given their ongoing and potential future contributions to sea-level rise. Numerical models of ice sheets are designed to simulate ice sheet behaviour in response to climate changes, but to be improved require validation against observations. The direct observational record of extant ice sheets is limited to a few recent decades, but there is a large and growing body of geochronological evidence spanning millennia constraining the behaviour of palaeo-ice sheets. Hindcasts can be used to improve model formulations and study interactions between ice sheets, the climate system and landscape. However, ice-sheet modelling results have inherent quantitative errors stemming from parameter uncertainty and their internal dynamics, leading many modellers to perform ensemble simulations, while uncertainty in geochronological evidence necessitates expert interpretation. Quantitative tools are essential to examine which members of an ice-sheet model ensemble best fit the constraints provided by geochronological data. We present an Automated Timing Accordance Tool (ATAT version 1.01) used to quantify differences between model results and geochronological-data on the timing of ice sheet advance and/or retreat. To demonstrate its utility, we perform three simplified ice-sheet modelling experiments of the former British-Irish Ice Sheet. These illustrate how ATAT can be used to quantify model performance, either by using the discrete locations where the data originated together with dating constraints or by comparing model outputs with empirically-derived reconstructions that have used these data along with wider expert knowledge. The ATAT code is made available and can be used by ice-sheet modellers to quantify the goodness of fit of hindcasts. ATAT may also be useful for highlighting data inconsistent with glaciological principles or reconstructions that cannot be replicated by an ice sheet model.

1 Introduction

Numerical models have been developed which simulate ice sheets under a given climate forcing (e.g. Greve, 1995; Rutt et al., 2009; Pollard and DeConto, 2009; Winkelmann et al., 2011; Gudmundsson et al., 2012; Cornford et al., 2013; Pattyn, 2017). When driven by future climate scenarios, these models are used to forecast the fate of the Antarctic and Greenland ice sheets (e.g. Seddik et al., 2012; DeConto and Pollard, 2016), providing predictions of their potential contribution to future sea level rise. However, incomplete knowledge of ice physics, boundary conditions (e.g. basal topography) and parameterisations of physical processes (e.g. basal sliding, calving), as well as the difficulty of predicting future climate, lead to uncertainty in these predictions (Applegate et al., 2012; Briggs et al., 2014; Ritz et al., 2015). Observations of ice marginal fluctuations (decades) and the processes of ice calving, flow or melting (subaerial or submarine) that facilitate or drive such variations, provide a powerful means to

understand the processes leading to the possibility of deriving new formulations that improve the realism of modelling. However, the short-time span (decades) of these observations limits their being used to constrain, initialise or validate modelling experiments (Bamber and Aspinall, 2013). Conversely, palaeo-ice sheets, especially from the last glaciation (~21,000 years ago), left behind evidence which provides the opportunity to study ice sheet variations across timescales of centuries to millennia, albeit with increased uncertainty in exact timing.

Numerous modelling studies have aimed to simulate the growth and decay of palaeo-ice sheets, producing hindcasts of ice-sheet behaviour (e.g. Boulton and Hagdorn, 2006; Hubbard et al., 2009; Tarasov et al., 2012; Gasson et al., 2016; Patton et al., 2016). Results from these hindcasts may be compared with empirical data recording ice sheet activity, so as to discern which parameter combinations produce results that best replicate the evidence of palaeo-ice sheet activity. Three classes of data are of particular use for constraining palaeo-ice sheets; (i) geomorphological data, (ii) relative sea level history, and (iii) geochronological data. Ideally, all three classes of data should be used to quantify the goodness of fit of a hindcast.

Geomorphological evidence comprises the landforms created by the action of ice upon the landscape, and can typically provide data on ice extent, recorded by moraines and other ice marginal landforms and on ice-flow directions recorded by subglacial landforms such as drumlins. Such landforms can be used to decipher the pattern of glaciation (e.g. Kleman et al., 2006; Clark et al., 2012; Hughes et al., 2014). Two tools have already been developed which can compare modelled ice margins and flow directions to the geomorphological evidence base (Napieralski et al., 2007).

Relative sea level data provides information regarding the mass-loading history of an ice sheet. Palaeo-ice-sheet model output is often evaluated against relative-sea-level data by use of glacio-isostatic adjustment models (e.g. Tushingham and Peltier, 1992; Simpson et al., 2009; Tarasov et al., 2012; [Auriac et al., 2016](#)).

Geochronological evidence attempts to ascertain the absolute timing of ice advance and retreat using dated material (e.g. organic remains dated by radiocarbon measurement) found in sedimentary contexts interpreted as indicating ice presence or absence nearby. It enables reconstruction of the chronology of palaeo-ice sheet growth and decay (Small et al., 2017) and is the underpinning basis for empirically-based ice sheet margin reconstructions (e.g. Dyke, 2004; Clark et al., 2012; Hughes et al., 2016). Although widely used in empirical reconstruction of palaeo-ice sheets, geochronological data has rarely been directly compared with ice sheet model output (although see Briggs and Tarasov, 2013). Such a comparison could be useful both for constraining ice-sheet model uncertainty and for identifying problems with the geochronological record. For example, a poor fit between model output and empirical data on timing could inform on the validity of a numerical model (or its parameterisation), or it could provide a physical basis for questioning the plausibility of empirically-driven interpretations or specific lines/data points of evidence given that they are associated with inherent uncertainties. In order to maximise the benefit to all users, any comparisons between palaeo-ice sheet model output and empirical data should ideally consider the inherent uncertainties of both.

Given the wide availability of compilations of geochronological data (e.g. Dyke, 2004; Hughes et al., 2011; Hughes et al., 2016), as well as the proliferation of ice sheet models (e.g. Greve, 1995; Rutt et al., 2009; Pollard and DeConto, 2009; Winkelmann et al., 2011; Gudmundsson et al., 2012; Cornford et al., 2013; Pattyn, 2017), a convenient, reproducible and consistent procedure for comparison should be of great utility to the palaeo-ice sheet community. The typical volume of geochronological constraints (several thousands) for a palaeo ice sheet and the

number of ensemble runs (several hundreds) from an ice sheet model make a visual matching of data and model output nearly impossible to accomplish, which is likely to explain the rarity of such comparisons. Here, we present an Automated Timing Accordance Tool (ATAT, version 1.01) ~~that compares geochronological data and ice-sheet model output.~~ ATAT a systematic means for comparing ice-sheet model output with geochronological data, which quantifies the degree of fit between the two. To separate model uncertainty from data error, a single run of ATAT focuses on the error in geochronological data. However, through multiple comparisons against an ice-sheet model ensemble which considers model uncertainty, ATAT could be used as a basis for examining whether model-data mismatch is a consequence of inadequacies in either the model or data. The tool is in the form of a Python script and requires the installation of open-source libraries. ATAT is written to handle NETCDF data as an input, a format commonly used in ice sheet modelling and is also accessible from many GIS packages in which geochronological data can be stored and manipulated.

2 Background

Geochronological evidence and ice sheet model outputs are often independently used to reconstruct the timing of glaciological events. The two approaches are fundamentally different in nature and consequently produce contrasting data outputs. Thus, before describing our approach to comparing the two sets of data (ATAT), we first consider the nature of both geochronological data and ice-sheet model output to highlight the issues and potential difficulties associated with comparing the two and conceptualise a comparison procedure.

2.1 Geochronological data

The timing of palaeo-ice sheet activity has primarily been dated using three techniques: (i) radiocarbon dating; (ii) cosmogenic nuclide exposure dating, and (iii) luminescence dating (Figure 1). The utility of each method for determining the timing of palaeo-ice sheet activity has been extensively reviewed elsewhere (e.g. Fuchs and Owen, 2008; Balco, 2011; Small et al., 2017) and only a brief description is provided here. Radiocarbon dating uses the known rate of the radioactive decay of ^{14}C to determine the time elapsed since the death of organic material (Libby et al., 1949; Arnold and Libby, 1951; Figure 1). For palaeo-glaciological purposes, the dated organic material (e.g. shells, mosses, plant remains) is usually taken from basal sediments overlying and closely associated with a glacial deposit in order to determine a minimum deglaciation age (e.g. Heroy and Anderson, 2007; Lowell et al., 2009); ice is interpreted to have retreated from this site some short time prior to this age. Where organic matter is either reworked within or is located directly beneath a glacial deposit, it can be used to constrain the maximum age of glacial advance (e.g. Brown et al., 2007; Ó Cofaigh and Evans, 2007); advance happened sometime after this age. Cosmogenic nuclides (e.g. ^{10}Be , ^{26}Al and ^{36}Cl) are produced by the interaction of secondary cosmic radiation in minerals, such as quartz, within materials exposed at the Earth's surface (Figure 1). Samples are generally taken from glacially-transported boulders, morainic boulders and glacially modified bedrock, all of which have ideally had signals from any previous exposure history removed by glacial erosion. Cosmogenic nuclide dating is thus used to determine the duration of time a sample has been exposed at the Earth's surface by determination of the concentration of cosmogenic nuclides within that sample. Luminescence dating can determine the age of a deposit by measuring the charge accumulated within minerals. This charge accumulates in light-sensitive traps within the crystal lattice due to ionizing radiation produced by

114 naturally occurring radioactive elements (e.g. U, Th, K). Luminescence dating determines the time elapsed since
 115 the last exposure of the mineral to sunlight; this exposure acts to reset the signal (Figure 1). As subglacial deposits
 116 are unlikely to have been exposed to light before burial, and therefore contain signals accumulated prior to
 117 deposition, luminescence dating within palaeo-glaciology is typically applied to ice marginal sediments, or those
 118 which overly glacial sediments (e.g. Duller, 2006; Smedley et al., 2016; Bateman et al., 2018). All
 119 geochronological techniques record the absence of grounded ice. They therefore provide either maximum or
 120 minimum ages of a glaciological event, depending upon the stratigraphic setting. Table 1 outlines a commonly
 121 used system used to classify geochronological data by stratigraphic setting (Hughes et al., 2011; 2016).
 122 The retreat/advance (ice-free) ages provided by the three geochronometric techniques are all affected by
 123 systematic and geological uncertainties (Small et al., 2017). Systematic uncertainties originate from the tools and
 124 techniques used to derive the date, such as laboratory instruments and sample preparation, and are accounted for
 125 in the quoted errors that accompany a date. Geological uncertainties are caused by the geological history of a
 126 sample, before, during and after a glacial event (e.g. Lowe and Walker, 2000; Lukas et al., 2007; Heyman et al.,
 127 2011). Such influences may leave little or no evidence of their effect upon a sample and are thus hard to quantify.
 128 The relationship between a dated sample and the glacial event it indicates is the largest potential source of
 129 uncertainty in geochronological data and is primarily bounded by the ability of the investigator to find and
 130 associate dateable material to the glacial event of interest. Since all geochronological techniques measure the
 131 absence of ice, expert inference must be made, and are influenced by the availability of information (stratigraphic
 132 or otherwise) at a study site; they may be open to change (e.g. new radiocarbon calibrations, new cosmogenic
 133 isotope production rates). Furthermore, in the cases of luminescence and radiocarbon dating, there can be an
 134 unknown duration since glacial occupation of an area and the deposition of dateable material. These factors mean
 135 it is necessary to consider the quality of dates for ascertaining the timing of the glacial event in question (Small et
 136 al., 2017).
 137 Numerous geochronological studies have sought to ascertain the timing of palaeo-ice sheet activity at sites, leading
 138 to compilations of geochronological data which bring together hundreds to thousands of published dates (e.g.
 139 Dyke et al., 2002; Livingstone et al., 2012; Hughes et al., 2011; 2016). Despite the growing number of reported
 140 dates, they are still insufficient in number and spatial spread to define, on their own, the time-space envelope of
 141 the shrinking ice sheet. Techniques to interpolate geochronological information between sites are required. The
 142 most commonly used technique is empirical ice sheet reconstruction (e.g. Dyke, 2004; Clark et al., 2012), whereby
 143 expert assessments of the geochronological and geomorphological record are used together to create ice-sheet
 144 wide isochrones of ice-sheet margin position and flow configuration. A recent advance in this method has been
 145 the inclusion of confidence envelopes for each isochrone, documenting possible maximum, likely and minimum
 146 extents (Hughes et al., 2016). Further techniques for spatiotemporally interpolating geochronological data include
 147 Bayesian sequence modelling (e.g. Chiverrell et al., 2013; Smedley et al., 2017), in which collections of deglacial
 148 ages are arranged in spatial order determined by a priori knowledge of geomorphologically-informed ice flow and
 149 retreat patterns (e.g. Gowan, 2013). Such techniques provide viable methods for producing ice-sheet wide
 150 chronologies, filling in information in locations where geochronological data may be sparse.

2.2 Ice sheet model output

Ice-sheet models solve equations for ice flow over a computational domain, for a given set of input parameters and boundary conditions, to determine the likely flow geometry and extent of an ice sheet. Typically, ice-sheet models run using finite difference techniques on regular grids (e.g. Rutt et al., 2009; Winkelmann et al., 2011). Ice-sheet models that utilise adaptive meshes (e.g. Cornford et al., 2013) and unstructured meshes also exist (e.g. Larour et al., 2012) and the results from such models can be interpolated onto spatially regular grids. The spatial resolution of an ice-sheet model depends upon the computational resources available, and the spatial resolution of available boundary conditions. Continental-scale models of palaeo-ice sheets have typical spatial resolution of tens of kilometres (e.g. Briggs and Tarasov, 2013; DeConto and Pollard, 2016; Patton et al., 2016), though parallel, high-performance computing means higher resolutions are possible (e.g. 5 km in Golledge et al., 2013 and Seguinot et al., 2016). The temporal resolution of ice sheet model output is ultimately limited by the time-steps imposed by the stability properties of the numerical schemes solving the ice-flow equations. Given that these stable time-steps can be sub-annual, output frequency is mostly predetermined by the user (typically decades to centuries), and as such is constrained by available disk-storage. Ice-sheet models therefore produce spatially connected predictions of ice-sheet behaviour such as advance and deglaciation (e.g. Table 1) across gridded domains at various temporal and spatial resolutions.

The stress fields imposed upon ice can be fully described by solving the Stokes equations. Indeed, ‘full Stokes’ models which do so have been tested (Pattyn et al., 2008) and used to simulate ice sheets (e.g. Seddik et al., 2012). However, fully solving the Stokes equations over the spatio-temporal scales relevant to palaeo-ice sheet researchers remains beyond the limit of currently available computational power. This problem is exacerbated by the need to run multi-parameter valued ensemble simulations to account for model uncertainty over multi-millennial and continental-scale domains. This means that palaeo-ice sheet modelling experiments rely upon approximations of the Stokes equations (see Kirchner et al., 2011 for a discussion), such as the shallow ice approximation (SIA) and shallow shelf approximation (SSA). The choice of ice-flow approximation used within a model has implications for the capability of models to realistically capture aspects of ice sheet flow (Hindmarsh, 2009; Kirchner et al., 2011; 2016), and in turn influences the nature of the model output produced. For instance, the SIA is not applicable for ice shelves, therefore SIA-based models do not produce modelled ice shelves (e.g. Glimmer; Rutt et al., 2009). Therefore, the timing of deglaciation in an SIA model can be determined as the point at which ice thickness in a cell becomes zero or thinner than the flotation thickness, ~~whereas in a SSA or higher-order model the location and movement of the grounding line must be determined. In a model which predicts the location of ice shelves (e.g. a SSA or higher-order model), the location and movement of the grounding line must be determined in order to calculate the modelled retreat or advance age. Such models typically produce a ‘mask’ variable from which the extent of grounded ice can be determined (e.g. PISM; Winkelmann et al., 2011).~~

Though ice sheet models produce output which is consistent with model physics, there are many sources of uncertainty involved with ice sheet modelling. This uncertainty has two main sources: (i) parameterisations, and (ii) boundary conditions. Where a process is too complex (e.g. calving) or occurs at too small a scale (e.g. regelation) to be captured by an ice sheet model, it is often simplified and parameterised. Associated with each parameterisation are a set of parameters, the values of which are either unknown, or thought to vary within some plausible bounds, ~~and. This leads to an associated uncertainty when choosing these input parameters,~~ which can either be constant or spatially and temporally variable across a domain. An example of a process which is often

parameterised is basal sliding. This parameterisation is often done through the implementation of a sliding law (e.g. Fowler, 1986; Bueler and Brown, 2009; Schoof, 2010), which relates the basal shear stress to the basal velocity (Fowler, 1986). ~~Exact determination of basal shear stress requires knowledge of basal roughness, hydrological conditions and, where present, sediment rheology. These terms~~ Parameters used to determine this relationship are often assigned or incorporated within a parameter, or prescribed by another model parameterisation (e.g. a subglacial hydrology model). Adding to the uncertainty in the absence of a single preferable sliding law, ice-sheet models often allow the user to choose between different sliding law implementations.

Boundary conditions, the values prescribed at the edge of the modelled domain, also introduce uncertainty into ice-sheet models. For contemporary ice sheets, there is a large uncertainty in the basal topography (e.g. Fretwell et al., 2013). This is less of a problem for the more accessible beds of palaeo-ice sheets. However, accurately accounting for the evolution of this bed topography over the course of a glaciation requires a model of isostatic adjustment (Lingle and Clark, 1985; Gomez et al., 2013).

A very large source of uncertainty for modelling palaeo-ice sheets is the climate used to drive them (Stokes et al., 2015), as indeed is the case for forecasts of contemporary ice sheets (e.g. Edwards et al., 2014). Owing to the computational resources required and technical challenges, few palaeo-ice sheet models are coupled with climate models. ~~This uncertainty over past climate is reflected in the large range of outputs produced by global circulation models which have tried to simulate the last glacial cycle (e.g. Braconnot et al., 2012).~~ Palaeo-ice sheet modellers have ~~mostly used offline methods to force their models with representations of palaeo-climate. used a range of methods to force their models, including~~ These include simple parameterisations (Boulton and Hagdorn, 2006), applying offsets derived from ice core records to contemporary climate (Hubbard et al., 2009) and scaling between present-day conditions and uncoupled global-circulation-model simulations at maximum glacial conditions (Gregoire et al., 2012; Gasson et al., 2016). Each approach ~~has advantages and disadvantages, but, most importantly, is also~~ associated with an inherent uncertainty. When this uncertainty is accounted for, the range of possible climates produces numerous ice sheet outputs.

There is another cause of ice-sheet models not being able to accurately predict the evolution of ice-sheets, which is the presence of instabilities – we use this term in the technical sense of a small perturbation in leads to the whole ice-sheet system amplifying this small perturbation to the extent it can leave a mark in the geological record. A classic example of this in ice-sheet dynamics is the marine ice-sheet instability (MISI), first discussed in the 1970s (Hughes, 1973; Weertman, 1974; Mercer, 1978) and more recently put on a sounder mathematical footing (Schoof 2007, 2012).

The MISI actually refers to an instability in grounding-line (GL) position on a reverse slope, where the water depth is shallowing in the direction of ice flow. Since ice flux increases with ice thickness, a straightforward argument leads to the conclusion that if the GL advances into shallower water, the efflux will decrease, the ice sheet will gain mass and the advance continue. If, on the other hand, the GL retreats, the efflux will increase, the ice-sheet will lose mass and the retreat continue. ~~The latter process led to concerns that the retreat of Antarctic and Greenlandic ice sheets would cause several metres of sea-level rise over one or two centuries. Schoof (2007,2012) showed that the MISI was in accordance with the understanding and use of the word ‘instability’ by physicists and mathematicians.~~

In principle, given the right parameterisations and basal topography, ice-sheet models should be able to predict the ‘trajectory’ of GL migration arising as a consequence of the MISI. However, the MISI is one of the class of instabilities that lead to poor predictability; certain small variations of parameters and specifications will lead to large-scale changes in the ‘trajectory’, in this case the retreat history. A well-known analogy is the ‘butterfly effect’, which originated in atmospheric modelling work (Lorenz, 1963); the butterfly effect is concerned with the consequences of the statement “small causes can have larger effects”. Recent work has also shown that additional physical processes, such as ice-shelf buttressing (Gudmundsson, 2012) and the effect that the gravitational pull of ice-sheets has on sea level (Gomez et al., 2012) have additional effects on grounding line stability. Given that most of the palaeo-ice sheets during the last glacial cycle had extensive marine margins and overdeepened basins, with isostatic adjustment creating further zones of reverse slope, capturing grounding line processes is important for simulating these ice-sheets.

~~Schoof’s theory was for a very straightforward marine ice-sheet configuration —no buttressing, ice motion all by sliding, isothermal, but its accuracy was confirmed by a large group of researchers running their models for this simple configuration (Pattyn et al., 2012). Schoof (2012) showed that for his configuration, the existence of a reverse slope was sufficient condition for the MISI to exist. However, later work (Gudmundsson, 2012; Gomez et al., 2012) presented results showing that stable GL positions could exist on a reverse slope if extra physical processes were included (Gudmundsson introduced buttressing, Gomez et al. included the effect of lateral gravitational attraction on sea-level). Their results indicated that the reverse slope was not a sufficient condition for instability.~~

~~Most of the palaeo-ice sheets at the LGM had extensive marine margins at their polar edges, certainly the Laurentide, Fennoscandian and British-Irish ice-sheets, and the present-day bathymetry of the seas around North America and Europe strongly suggests that a reverse slope would have existed —moreover, isostatic adjustment under the weight of the ice-sheets would have created further extensive zones of reverse slope. There are data indicating rapid retreat along some zones of reverse slope in palaeo-ice sheets, which leads to the question of how accurately we should expect ice-sheet models to be able to reproduce the observed retreat rates in the presence of physical instability. Schoof’s progress is very recent, so the necessary ensemble runs have yet to be carried out by researchers focussing on the relationship between the presence of the MISI and the amplification of data uncertainties or physics errors/over-simplifications (as placed in the models).~~

2.3 Considerations when comparing geochronological data and ice-sheet model output

Sections 2.1 and 2.2 make it clear that several factors must be considered in order to satisfactorily compare geochronological data and ice-sheet model output (Table 2). Most critically, the two datasets involved in any comparison have varying spatial properties. Raw geochronological data is unevenly distributed and located at specific points, with horizontal position accurate to a metre or so; such data may be used to plot ice-margin fluctuations of the order of tens of kilometres (Figure 2C). Ice-sheet models typically produce results on evenly-spaced points (at ~5 km to 20 km resolution) that are distributed over and beyond the maximum area of the palaeo-ice sheet (Table 2; Figure 2B). Consequently, in comparing the two, a choice must be made; either geochronological data should be gridded (coarsened) to the resolution of the ice-sheet model, or the ice-sheet model results must be interpolated to a higher resolution. Both options have drawbacks, as the former removes spatial accuracy from geochronological data while the latter relies upon interpolation beyond model resolution

269 and, more seriously, model physics. A second problem lies in the spatial organisation of the data (Table 2). Ice-
 270 sheet models produce a regular grid of data (Figure 2B), meaning that no location is more significant than any
 271 other when comparing the modelled deglacial chronology with that inferred from geological data. Conversely,
 272 owing to the uneven distribution of raw geochronological data, some regions of a palaeo-ice sheet may be better
 273 constrained than others (Figure 2C). As noted by Briggs and Tarasov (2013), any comparison that does not treat
 274 the uneven spatial distribution of geochronological data may favour sites where numerous dates exist over more
 275 isolated locations. One approach to overcoming these disparities is to use an interpolation scheme (e.g. empirical
 276 reconstruction, Bayesian sequence) on the raw geochronological data. This produces a geochronological
 277 framework by combining evidence on pattern and timing to yield a distribution that is spatially more uniform and
 278 a spatial resolution similar to that of palaeo-ice sheet model output (Figure 2D).
 279 The temporal intervals between and precision of geochronological data and ice sheet model output also vary
 280 (Table 2). The time intervals between geochronometric data are determined by the number of available
 281 observations, and precision determined by sources of uncertainty. Conversely, ice sheet models produce output at
 282 regular intervals and are temporally exact, which is to be contrasted with ‘correct’. Since the output interval of an
 283 ice-sheet model is generally determined by the user (see Section 2.2) it is pertinent to consider an appropriate
 284 time-interval of ice-sheet model output for comparison with geochronological data. For example, radiocarbon
 285 dates have precision typically in the order of hundreds of years but do not directly constrain ice extent, whilst
 286 empirically reconstructed isochrones are typically produced for thousand-year time-slices (e.g. Hughes et al.,
 287 2016). In reality, ice-sheets may respond to events at faster time-scales than this, but in the absence of internal
 288 instabilities (e.g. MISI) palaeo-ice sheet models are ultimately limited by the temporal resolution of the available
 289 climate forcing data. Thus, to gain insight into controls on palaeo-ice sheet behaviour, it may be necessary to
 290 create model output with a greater (centurial) temporal resolution than the uncertainty associated with
 291 geochronology.
 292 Both geochronological data and ice-sheet model output have sources of uncertainty which must also be considered
 293 when comparing the two. For geochronological data, uncertainty is typically expressed as a standard deviation
 294 from the reported age, and are therefore easy to consider when comparing to an ice sheet model. For ice-sheet
 295 models, individual model runs do not currently express uncertainty, and it is only when multiple, ensemble, runs
 296 which systematically vary parameters and boundary conditions are conducted that uncertainty in all output
 297 variables can be expressed. Having said this, statistical techniques exist to derive probability distribution functions
 298 for individual quantities (e.g. Ritz et al., 2015). Such ensemble runs typical comprise hundreds to thousands of
 299 individual runs (Tarasov and Peltier, 2004; Robinson et al., 2011). Given the volume of data this produces, one
 300 appealing application of a quantitative comparison between geochronological data and ice sheet model output
 301 would be to act as a filter for scoring ice-sheet model runs and reducing predictive uncertainty by only using the
 302 parameter combinations that were successful. However, if all possible parameters have been modelled, (i.e. the
 303 full ‘phase-space’ of the model has been explored (cf. Briggs and Tarasov, 2013)), and very few (or no) model
 304 runs conform to a certain set of geochronological data or an empirical reconstruction, this may provide a basis to
 305 question aspects of the evidence (e.g. re-examining the stratigraphic context of a dated sample site or questioning
 306 the basis of the reconstructed isochrone). Of course, a third possibility that both data and model are incorrect
 307 cannot be excluded.

308 We therefore suggest that any comparison between ice-sheet model experiments and geochronological data should
309 consider:

- 310 i) That both ice-sheet models and geochronological data have inherent uncertainties;
- 311 ii) That geochronological data typically provide a constraint on just the absence of ice; such that ice must have
312 withdrawn from a site sometime (50 years? 500 years? 5000 years?) prior to the date (which can be any point
313 within the full range of the stated uncertainty). It is thus a limit in time and not a direct ~~fix~~measure of glacial
314 activity. Figure 3 illustrates this for advance and retreat constraints. It is most often the case that dated material is
315 taken close to the stratigraphic boundary or landform representing ice presence, in which case a date might be
316 considered as a ‘tight constraint’ (e.g. the ice withdrew and very soon afterwards (50 years) marine fauna colonised
317 the area and deposited the shells used in dating). Sometimes however there may have been a large (centuries to
318 millennia) interval of time between the withdrawal and the age of the shell chosen as a sample, in which case the
319 date will provide a ‘loose’ limiting constraint; it might be much younger than ice retreat (Figure 3).
- 320 iii) There is inherent value to the expert interpretation of stratigraphic and geomorphological information, meaning
321 an ice-free age reported for a site is likely as close as possible (tight constraint) to a glacial event. However, this
322 interpretation could be subject to change;
- 323 iv) Geochronological data exist as spatially distributed dated sites (e.g. Figure 2C) which can be built into a
324 spatially coherent reconstruction (e.g. Figure 2D);
- 325 v) A great input uncertainty in a palaeo-ice sheet model is the climate, which can lead to changes in the spatial
326 extent and timing of ice sheet activity.
- 327 vi) A factor which requires further investigation is the relationship between the operation of a physical instability
328 (e.g. the MISI) and the practical ability of models to predict retreat or advance rates; the presence of an instability
329 can result in extreme sensitivity to parameter ignorance or over-simplified model physics.
- 330 vii) Other uncertainties can also lead to variations in ice-sheet model results; these can be accounted for in an
331 ensemble of hundreds to thousands of simulations.

332 Given the above, it is unlikely that a single procedure could capture model-data conformity. ATAT therefore
333 implements several ways of measuring data-model discrepancies and produces output maps (described in the
334 following two sections) to help a user assess which model runs best agree with the available geochronological
335 data. One approach is to transform the geochronological data points (x,y,t) to a gridded field (raster) that define
336 age constraints of ice advance and another grid for retreat. Both of these data types also require an associated grid
337 that reports the uncertainty range as error (Figure 4). These age grids may then be quantitatively compared to
338 equivalent grids (age of advance grid and age of retreat grid) derived from the ice sheet model outputs.
339 Alternatively, one might prefer to compare model runs against the geochronological data (points) combined with
340 expert-sourced interpretive geomorphological and geological data, in which age constraints from dated sites have
341 been spatially extrapolated using moraines and the wider retreat pattern. In this case ATAT allows the model
342 outputs to be compared to the ‘lines on maps’ type of reconstruction subsequent to conversion from age isolines
343 to a grid of ages (Figure 4).

3. Description of tool

ATAT is written in Python, and utilises several freely available modules. Access to these modules may require a Python package manager, such as 'pip' or 'anaconda'. ATAT can therefore be run from the command line on any operating system, or by using a Python interface such as IDLE.

3.1 Required data and processing

ATAT requires two datasets as an input: (i) an ice-sheet model output; and (ii) gridded geochronological data. Table 3 provides the required variables and standard names for each dataset. In order to determine the advance age or deglacial age predicted by the ice sheet model, ATAT requires either an ice thickness (where the model does not produce ice shelves) or a grounded ice-mask variable (where ice shelves are modelled). In the latter case, the user is asked to define the value which represents grounded ice.

Empirical advance and deglacial geochronological data (Table 1) require separate input files (NETCDF format), as model-data comparison for these two scenarios are run separately in ATAT. Table 1 and further references (Hughes et al., 2011; 2016; Small et al., 2017), provide information regarding identification of the stratigraphic setting of these two glaciological events as considered by ATAT. ATAT requires that geochronological data (advance or deglacial) are interpolated onto the same grid projection and resolution as the ice-sheet model before use. Though an imperfect solution to the problem of comparing grids of different resolution, (Section 2.3; Table 2), this was preferred to the alternative solution of regridding an ice sheet model onto a higher resolution grid, as this may introduce the false impression of high resolution modelling sensitive to boundary conditions (e.g. topography) beyond the actual model resolution.

Preparation of the geochronological data to be the same format and grid resolution as the ice sheet model output requires use of a GIS software package such as ESRI ArcMap or QGIS. Users must define deglacial/advance ages based either upon the availability of geochronological data in a cell, or based upon an empirical reconstruction (Figure 4). These ages must be calibrated to a calendar which is the same as that output by the ice-sheet model (in our case the 365-day calendar in units of seconds since 1-1-1). Where there are no data (i.e. outside the ice-sheet limit), the grid value must be kept at 0. When multiple dates are contained within a cell, expert judgement is required to ascertain which date is most representative of the deglaciation of a region. The assembly of this geochronological database input into ATAT should consider the reliability of ages, removing outliers and unreliable ages (see Small et al. (2017) for a discussion of this issue). In a comparable manner, the attribution of error to each cell is also reliant upon expert interpretation. The magnitude of error may vary between the source of geochronological data and user choice for experimental design (e.g. 1, 2 or 3 sigma). A single error value must be given for each dated cell, corresponding to the maximum threshold beyond which it is unacceptable for a model prediction to occur (Figure 3). Given that ~~this creating this input data~~ may involve many expert decisions (e.g. which date has the relevant stratigraphic setting, which date(s) are most reliable?), this part of the process is not yet automated within ATAT. This data preparation stage is therefore the most time-consuming and user-intensive part of the process. However, users only need to define the data-based advance/deglacial grid once to compare to multiple model outputs. Future work should consider alternatives means of choosing dates and identifying outliers, such as Bayesian age modelling (e.g. Chivverell et al., 2013). The input data NetCDF file should also contain the variables latitude, longitude, base topography (the topography that the ice-sheet modelling is conducted on and the elevation of the geochronological sample (Table 3).

ATAT is called from a suitable python command-line environment, using several system arguments to define input variables. Upon starting ATAT, the user is first asked to define whether they are testing a deglacial or advance scenario (Table 1; Figure 5). Users must define whether they are testing a deglacial or advance scenario. ATAT only considers the last time that ice advances over an area. Therefore, caution must be undertaken when defining advance data in regions where multiple readvances occur, and users should consider limiting the time interval of the ice sheet model tested when examining specific events (e.g. a well-dated readvance or ice sheet build-up). The location of the file containing the geochronological data grid (e.g. Figure 5) is then required. From this file, the age and error grids are converted to arrays. For the age data, null values are masked out using the numpys masked array function. A second array that accounts for error is then created, the properties of which depends upon whether a deglacial or advance scenario is being tested. For a deglacial scenario, a model prediction will be unacceptable if the cell is ice-covered after the range of the date error is accounted for, but the cell may become deglacialated any time before this. Therefore, the associated error value is added onto the cell date, to create a maximum age at which a cell must be deglacialated by to conform to the ice sheet model (Figure 3). The opposite is true for advance ages; ice can cover a cell any time after the date and associated error, but cannot cover the cell before the date of the advance. In order to allow for advances which occur after the date and its error, associated error is therefore subtracted from the date cell (Figure 3). To account for the uneven spatial distribution of dates, a weighting for each date is then calculated based upon their spatial proximity. This weighting is used later when comparing the data to the model output. To calculate this weighting (w_i), ATAT defines a local spatial density of dated values based upon a kernel search of 10 neighbouring cells. the Euclidian distance from each dated cell to its nearest dated cell (d_i) is calculated. The mean distance between dated cells (\bar{d}) is then calculated, and the weight of each location (w_i) defined using Eq. (1):

$$w_i = \sqrt{\frac{d_i}{\bar{d}}}, \quad (1)$$

The user is then asked to define the path to the ice sheet model output, from which the modelled deglacial age will be calculated and eventually compared to the data (Figure 4). The user must also define whether to base deglacial timing on an ice thickness or grounded extent mask variable (Table 2). If the user selects thickness, the margin is defined by an increase from 0 ice thickness. For the mask, the user is also asked to supply the number which refers to grounded ice extent. The timing of advance is then determined by the change of a cell to this number (Figure 5). The margin position recreated by the ice-sheet model has a spatial uncertainty due to downscaling issues and fluctuations which may occur between recorded outputs. To account for this, ATAT calculates a second set of modelled deglacial ages, whereby the deglacialated region at each modelled time output is expanded to all cells which neighbour the originally identified deglacialated or advanced over cells. Furthermore, the spatial resolution of ice-sheet models typically means that the emergence of ice-free topography at the edge or within an ice-sheet (e.g. in situations such as steep-sided valleys or nuntaks) are poorly represented. To account for this, ATAT firstly calculates the modelled ice-sheet surface at each time output by adding ice thickness to the input base topography. Where the modelled surface elevation is below that of the sample elevation, these cells are identified as being deglacialated (Figure 5). The downscaling of topography onto ice-sheet model grids also introduces a vertical uncertainty. This is accounted for in ATAT through calculating the difference between sample elevation and the reference elevation. A second metric which identifies cells as having been deglacialated if they are also within this vertical uncertainty is also calculated (Figure 5).

Formatted: Space Before: 0 pt, After: 0 pt

3.2 Model-data comparison

Once the required variables have been retrieved from the NETCDF data and manipulated, ATAT compares the geochronological age and modelled age at each location (Figure 4). Firstly, the grid cells which have data are categorised as to whether there is model-data agreement, based on the criteria shown in Figure 3. Since all dating techniques only record the absence of ice, geochronological data provides only a one-way constraint on palaeo-ice sheet activity. For deglacial ages, deglaciation could occur any time before the geochronological data provided and within the error of the date, but deglaciation must not occur after the error of the date is considered (Figure 3). For advance ages, advance must have happened after the date or within error beforehand, but palaeo-ice sheet advance cannot occur in the time period before that dated error (Figure 3). Once ATAT has determined whether each cell conforms to these criteria, a map is produced identifying at which locations the ice sheet model agrees with the geochronological data.

Though the criteria described above and illustrated in Figure 3 allow for the identification of dates which conform to the predictions of an ice sheet model, they provide little insight into how close the timing of the model prediction is to the geochronological data. If these were the only criteria on which a model-data comparison was made, it could prove problematic. In an extreme case, one could envisage that all retreat dates are adhered to by a model run that deglaciates from a maximum extent implausibly rapidly (say 50 years!), and, given that we only have one-way constraints on deglaciation (Figure 3), this model run would conform to all modelled dates. Whilst the nature of geochronological data (being only able to determine the absence of ice) does not preclude such a scenario, this assumes that there is no inherent value to the expert judgement and stratigraphic interpretation of each date as being close to palaeo-ice sheet timing (cf. Small et al. 2017). Therefore, ATAT also determines the temporal proximity of the geochronological data and the model prediction. Firstly, a map of the difference between modelled and empirical ages is created (Figure 5). This enables the identification of dates which are a large distance away from the model prediction. Secondly, the route-mean square error (RMSE) is calculated using the Eq. (2):

$$RMSE = \sqrt{\frac{1}{n} \sum_{i=1}^n (g_i - m_i)^2}, \quad (21)$$

where n is the number of cells which contain empirical geochronological information, g_i is the associated geochronological date, and m_i is the model predicted age. The RMSE works well when the geochronological data is evenly spatially distributed, either from a reconstruction (i.e. isochrones) or a wealth of dates. ATAT also calculates a weighted RMSE (wRMSE), for situations where this is not the case (i.e. there is a paucity of dates that are not distributed evenly across the domain) using Eq. (3):

$$wRMSE = \sqrt{\frac{1}{n} \sum_{i=1}^n ((g_i - m_i) * w_i)^2}, \quad (22)$$

where w_i is the spatial weighting factor, determined in Eq. (1). Both the RMSE and wRMSE are calculated for all dates, to create a metric that doesn't account for dating error but may give an indication of how close a model-run gets to dated cells, and also for those dates which where model-data agreement within dating error occurs to create a metric which does account for model-error dated regions which have different levels of conformity with

Formatted: Subscript

the model output (Figure 5). ATAT then produces a .csv file containing all calculated with these statistics per ice-sheet model output file. Given the complexity of data-model comparison, different statistics may have different uses. For instance, the percentage of covered dates may prove useful to identify the worst performing model runs (i.e. the bottom 50%) as a first filter of model runs, whilst the wRMSE of dates within error may be more convenient for choosing between filtered model runs. However, given the uncertainty in ice-sheet modelling it is likely that in an ensemble there will be no single model run which has significantly better metrics than others, so ATAT may best be used to choose members which pass a user-defined threshold of combined metrics.

4. Application of tool

4.1 Ice Sheet Model

To trial ATAT we used geochronological data and ice sheet modelling experiments from the former British-Irish Ice Sheet (BIIS). A vast quantity of previous research has produced a high density of dates (Hughes et al., 2011) which are being substantially augmented by the BRITICE-CHRONO project (<http://www.britice-chronology.group.shef.ac.uk/>). Along with an abundance of well documented landforms (Clark et al., 2017), this makes the BIIS a data-rich study area for empirical reconstructions and ice sheet modelling. Ongoing modelling work aims to capture the behaviour of the BIIS inferred from the geomorphological and geochronological record (see Clark et al., 2012 for a recent reconstruction). We do not expect our model to capture these specific details. Instead, the purpose of modelling in this paper is merely to illustrate the use of ATAT. We therefore restrict ourselves to simplified modelling experiments and show only three model runs (Experiments A, B and C), whereas a full ensemble experiment would contain hundreds or thousands of simulations.

Ice sheet modelling experiments were conducted using the Parallel Ice Sheet Model (PISM; Winkelmann et al., 2011). This is a hybrid SIA-SSA model, with an implementation of grounding line physics. It is therefore suited to modelling both the marine-based portions of the BIIS and the terrestrial realm. The model simulates the history of the BIIS from 40 ka to present. The model is run at 5 km resolution, with basal topography derived from the General Bathymetric chart of the Oceans (www.gebco.net). This is updated to account for isostatic adjustment using a viscoelastic Earth model (Bueler et al., 2007) and a scalar eustatic sea level offset based on the SPECMAP data (Imbrie et al., 1984). All three model runs, labelled A-C, had the same input parameters and boundary conditions, apart from climate forcing. We take a similar approach to Seguinot et al. (2016) in computing a climate forcing. Modern values of temperature and precipitation are perturbed by a proxy temperature record, in this case the GRIP ice core record (Johnsen et al., 1995). These are input into a positive degree day model to calculate mass balance (Calov and Greve, 2005). Input precipitation values are the same between experiments. To introduce variation between the experiments, temperature varies such that Experiment A is the equivalent of modern day values, Experiment B has values uniformly reduced by 1°C and Experiment C has values uniformly reduced by 2°C. All other parameters and forcings are equal between experiments. This simple approach to climate forcing here used for demonstration purposes only, and does not capture the changes to atmospheric and oceanic circulation patterns that occur during a glacial cycle.

The maximum extent of ice for each experiment is shown in Figure 6 and the timing of advance and retreat is shown in Figure 7. Potentially unrealistic ice sheets occur in the North Sea, perhaps due to the choice of domain not including the influence of the Fennoscandian ice sheet in this area. As noted above, we do not expect these

model runs to fully replicate the reconstructed characteristics of the BIIS (e.g. Clark et al., 2012). However, it is worth noting general, visually-derived, observations regarding the outputs shown in Figure 6. For larger temperature offsets, the ice sheet gets bigger, the timing of maximum extent gets progressively later and the modelled ice sheet gets thicker (Figure 6). In all experiments, there is generally a gradual advance toward the maximum extent followed by retreat (Figure 7). This pattern is interrupted by a later readvance that corresponds to the timing of the Younger Dryas in the GRIP record; this causes ice to regrow over high elevation areas such as Scotland and central Wales. The extent of this readvance increases with decreased temperature offsets between experiments (Figure 7). Smaller readvances, occurring around 16.5 ka also occur (Figure 7).

4.2 Geochronological data

Ice-sheet advance dates were taken from the compilation of Hughes et al. (2016) and gridded to the ice sheet model domain (Figure 4). In total, 61 cells were represented with advance dates (Figure 8A). Considering now ice-sheet retreat (Figure 8B), dates deemed reliable or probably reliable by Small et al. (2017) were used (i.e. those given a ‘traffic light rating’ of green or amber). For the dated advance and retreat locations, the geochronological data in each cell was assigned an error corresponding to that which was reported in the literature. We also compared our results to the ‘likely’ empirical reconstruction of Hughes et al. (2016), based on that of Clark et al. (2012) (Figure 8C), using the minimum and maximum bounding envelopes to assign an error to each cell of the ice sheet grid (Figure 8D). The largest errors occur in the North Sea region, where there is a lack of empirical data (e.g. Figures 8A and B).

4.3 Results

Table 4 shows selected statistics derived by ATAT when comparing the three ice-sheet modelling experiments (Figures 6 and 7) against the three categories of data (Advance, Retreat, Isochrones; Figure 8). wRMSE was not calculated for the DATED isochrone reconstruction, as grid points are distributed evenly and therefore have equal spatial weighting (Table 4). Experiment C produces modelled ice-sheets with the greatest areal extent, and therefore performs best at correctly covering the dated areas (Table 4). However, none of the three experiments perform particularly well when compared with the data or the empirical reconstruction regarding timing and results in high (>2000 year) RMSEs (Table 4). The application of ATAT and the results from these simplified experiments allow us to suggest directions for analysing future experiments.

All three experiments produced large RMSEs, in the order of thousands of years, when compared to all three categories of data (Table 4). For advance ages, the three simulations conform to a large number of dated locations (e.g. 72% of ages in Experiments B and C; Table 4). However, the RMSEs of advance ages are high (Table 4). This shows that, while the models perform well at matching the constraint of covering an area in ice after an advance age (Figure 3), the models often glaciates a region much later than required. Advance dates are particularly difficult to obtain from the stratigraphic record, and often there may be a long hiatus between the initial deposition of datable material and the subsequent advance of a glacier. Future experiments with large ensembles should therefore consider the number of advance dates conformed to (rather than the RMSE) as a more robust guide for model performance during ice advance.

For the retreat comparisons, the three modelling experiments conform to a larger percentage of sites, seemingly outperforming the empirically-derived DATED reconstruction (Table 4). However, where model-data agreement

occurs, the RMSE produced are much higher when ~~for~~ the model is compared to the DATED reconstruction. This is due to the reconstruction containing large uncertainties in regions which lack geochronological control (for example in the North Sea, Figure 8). These uncertainties, a product of spatial interpolation across regions with sparse information, are much greater than those associated with individual dates. Figure 9A shows examples of output maps from ATAT which display the spatial pattern of agreement and the magnitude of the difference between Experiment C and the DATED reconstruction. This shows that due to the uncertainty associated with North Sea glaciation, even where the model produces an unrealistic artefact, there is data-model agreement. Furthermore, ATAT produces a map which displays the number of years between data-based and modelled retreat and/or advance (e.g. Figure 9B). Figure 9B, which compares Experiment C to the DATED isochrones, shows that the timing of model-data disagreement is spatially variable. If more modelling simulations were conducted, such maps may reveal regions of reconstruction or particular dates which are difficult to simulate in the model. In such cases, data or model re-evaluation may be required and herein lies the potential utility of this ATAT tool in making sense of ensemble model runs. However, such model-data comparison awaits a full-ensemble simulation which accounts for model uncertainty (e.g. Hubbard et al., 2009).

5. Summary and concluding remarks

Here we present ATAT, an automated timing-accordance tool for comparing ice-sheet model output with geochronological data and empirical ice sheet reconstructions. We demonstrate the utility of ATAT through three simplified simulations of the former British-Irish Ice Sheet. Note that a ~~fuller-larger~~ ensemble model of hundreds to thousands of runs is required for ~~full~~-model evaluation (e.g. Hubbard et al., 2009). ATAT enables users to quantify the difference between the simulated timing of ice sheet advance and retreat and those from a chosen dataset, and allows production of cumulative ice coverage agreement maps that should help distinguish between less and more promising runs. We envisage that this tool will be especially useful for ice-sheet modellers through justifying model choice from an ensemble, quantifying error and tuning ice-sheet model experiments to fit geochronological data. Ideally, this tool should be used in combination with other evaluation methods, such as fit to relative sea-level records. In the case where locations or regions of data cannot be fit by a model, and all model uncertainty has been accounted for in an ensemble simulation, the comparisons made in ATAT may also highlight that data re-evaluation is necessary. ATAT is supplied as supplementary material to this article.

6. Code Availability

ATAT 1.0-1 source code is freely distributed under a GNU GPL licence as supplementary material to this paper and can be downloaded from <https://figshare.com/s/38d0fd268684ad0fcc2d>. An example geochronological data grid can also be downloaded as supplementary material. The ice sheet modelling experiments shown here were conducted using the Parallel Ice Sheet Model (<http://pism-docs.org/>). Development of PISM is supported by NASA grant NNX17AG65G and NSF grants PLR-1603799 and PLR-1644277. The geochronological data used is freely available from <https://www.sciencedirect.com/science/article/pii/S0012825216304408#s0105> and <https://doi.pangaea.de/10.1594/PANGAEA.848117>.

6.1. General Instructions

ATAT is written in python, and distributed as both .py script, for use in Python 2, and a .py3 script, for use with Python 3. The tool requires installation of Python and the following freely available Python packages:

- netCDF4 (<https://pypi.python.org/pypi/netCDF4>)
- numpy (<http://www.numpy.org/>)
- scipy (<https://www.scipy.org/>)
- matplotlib (<https://matplotlib.org/>)
- matplotlib toolkit basemap (<https://matplotlib.org/basemap/>)

ATAT can be run from any Python enabled environment (e.g. IDLE, BASH). Here we provide the following simple instructions for running ATAT in a BASH shell. For numerous runs, a shell script should be created. Each stage has error reporting.

1. Open a BASH terminal and navigate to the directory containing the ATAT script (e.g. “cd /home/ATAT”).
2. From the command line, launch the ATAT script using python (“python ATATv1.01.py”). Eight command-line arguments (A1 - A8), separated by a space should then follow.

A1: A command-line prompt will ask whether dictates whether deglacial or advance ages are being tested. Type “DEGLACIAL” or “ADVANCE” accordingly, and press return.

4. A2 is the second prompt will ask for the path to the geochronological data file, type this in and press return (e.g. “/home/ATAT/geochron.nc”)

A3 defines the user whether the model extent is based on thickness or a mask. Type THK or MSK accordingly.

A4 5. is the The user is then asked to specify the path to the ice-sheet model output file (e.g. “/home/ATAT/icesheetmodel1.nc”)

6. A command line prompt will then ask the user whether the model extent is based on thickness or a mask. Type THK or MSK accordingly. In the case of MSK, the user is asked to define the numeric value of mask which represents grounded ice.

A5 is the value of the ice-sheet output mask. A value is required even if A3 = THK, but can be any value as it will be ignored.

A6 to A8 control output maps. A6 defines whether the output map should consider margin uncertainty, with a value of BORDER or NONE.

A7 defines whether the model-data offset map displaces RMSE (option “NONE”) or wRMSE (“WEIGHTED”).

A8 specifies which dates are plotted on the difference map, and can be “ALL” for all dates, “COVERED” for those which at some point were covered by ice and “INERROR” to display only those dates where model-data agreement within dating error occurred.

An example command would be “python ATATv1.1.py DEGLACIAL /home/ATAT/dated_recon.nc MSK /home/ATAT/experiment1.nc 2 BORDER WEIGHTED INERROR”.

7.

ATAT then outputs the two maps and a csv table containing all derived statistics.

The user is then asked to define variables related to the output maps. For the model-data offset map (Figure 9B), either RMSE (type “NONE”) or wRMSE (type “WEIGHTED”) can be displayed for each site. For the cumulative

Formatted: Indent: First line: 0 cm

agreement map (Figure 9A), all sites (type “ALL”), those that the model glaciates at some point (type “COVERED”) or those that agree within error (type “INERROR”) can be displayed.
 8. ATAT then prints all statistics for the data-model comparison conducted to a .csv file, default name “ATAT_output.csv”.

Acknowledgements: This work was supported by the Natural Environment Research Council consortium grant; BRITICE-CHRONO NE/J009768/1. We thank Evan Gowan and Lev Tarasov for their constructive reviews which improved the manuscript.

References

- Auriac, A., Whitehouse, P.L., Bentley, M.J., Patton, H., Lloyd, J.M. and Hubbard, A. Glacial isostatic adjustment associated with the Barents Sea ice sheet: a modelling inter-comparison. *Quaternary Science Reviews*, 147, 122-135, 2016.
- Applegate, P.J., Kirchner, N., Stone, E.J., Keller, K. and Greve, R. An assessment of key model parametric uncertainties in projections of Greenland Ice Sheet behavior. *Cryosphere*, 6(3), 589-606, 2012.
- Arnold, J.R. and Libby, W.F. Radiocarbon dates. *Science*, 113(2927), 111-120, 1951.
- Balco, G. Contributions and unrealized potential contributions of cosmogenic-nuclide exposure dating to glacier chronology, 1990–2010. *Quaternary Sci Rev*, 30(1), 3-27, 2011.
- Bamber, J.L. and Aspinall, W.P.. An expert judgement assessment of future sea level rise from the ice sheets. *Nat Clim Change*, 3(4), 424-427, 2013.
- Bateman, M.D., Evans, D.J., Roberts, D.H., Medialdea, A., Ely, J. and Clark, C.D., The timing and consequences of the blockage of the Humber Gap by the last British– Irish Ice Sheet. *Boreas*, 47(1), 41-61, 2018.
- Boulton, G. and Hagdorn, M. Glaciology of the British Isles Ice Sheet during the last glacial cycle: form, flow, streams and lobes. *Quaternary Sci Rev*, 25(23), 3359-3390, 2006.
- Braconnot, P., Harrison, S.P., Kageyama, M., Bartlein, P.J., Masson-Delmotte, V., Abe-Ouchi, A., Otto-Bliesner, B. and Zhao, Y., 2012. Evaluation of climate models using palaeoclimatic data. *Nature Climate Change*, 2(6), 417-424, 2012.
- Briggs, R.D. and Tarasov, L. How to evaluate model-derived deglaciation chronologies: a case study using Antarctica. *Quaternary Sci Rev*, 63, 109-127, 2013.
- Briggs, R.D., Pollard, D. and Tarasov, L. A data-constrained large ensemble analysis of Antarctic evolution since the Eemian. *Quaternary Sci Rev*, 103, 91-115, 2014.
- Brown, E.J., Rose, J., Coope, R.G. and Lowe, J.J. An MIS 3 age organic deposit from Balglass Burn, central Scotland: palaeoenvironmental significance and implications for the timing of the onset of the LGM ice sheet in the vicinity of the British Isles. *J Quaternary Sci*, 22(3), 295-308, 2007.
- Bueler, E.D., Lingle, C.S. and Brown, J. Fast computation of a viscoelastic deformable Earth model for ice-sheet simulations. *Ann Glaciol*, 46(1), 97-105, 2007.
- Bueler, E. and Brown, J. Shallow shelf approximation as a “sliding law” in a thermomechanically coupled ice sheet model. *J Geophys Res-Earth*, 114(F3), 2009.

646 Calov, R. and Greve, R. A semi-analytical solution for the positive degree-day model with stochastic temperature
647 variations. *J Glaciol*, 51(172), 173-175, 2005.

648 Chiverrell, R.C., Thrasher, I.M., Thomas, G.S., Lang, A., Scourse, J.D., van Landeghem, K.J., Mccarroll, D.,
649 Clark, C.D., Cofaigh, C.Ó., Evans, D.J. and Ballantyne, C.K. Bayesian modelling the retreat of the Irish Sea Ice
650 Stream. *J Quaternary Sci*, 28(2), 200-209, 2013.

651 Clark, C.D., Hughes, A.L., Greenwood, S.L., Jordan, C. and Sejrup, H.P. Pattern and timing of retreat of the last
652 British-Irish Ice Sheet. *Quaternary Sci Rev*, 44, 112-146, 2012.

653 Cornford, S.L., Martin, D.F., Graves, D.T., Ranken, D.F., Le Brocq, A.M., Gladstone, R.M., Payne, A.J., Ng,
654 E.G. and Lipscomb, W.H. Adaptive mesh, finite volume modeling of marine ice sheets. *Journal of Computational*
655 *Physics*, 232(1), 529-549, 2013.

656 DeConto, R.M. and Pollard, D. Contribution of Antarctica to past and future sea-level rise. *Nature*, 531(7596),
657 591-597, 2016.

658 Duller, G.A.T. Single grain optical dating of glacial deposits. *Quaternary Geochronology*, 1(4), 296-304, 2006.

659 Dyke, A.S. An outline of North American deglaciation with emphasis on central and northern Canada.
660 *Developments in Quaternary Sciences*, 2, 373-424, 2004.

661 Dyke, A.S. An outline of North American deglaciation with emphasis on central and northern Canada.
662 *Developments in Quaternary Sciences*, 2, 373-424, 2004.

663 Edwards, T.L., Fettweis, X., Gagliardini, O., Gillet-Chaulet, F., Goelzer, H., Gregory, J.M., Hoffman, M.,
664 Huybrechts, P., Payne, A.J., Perego, M. and Price, S. Effect of uncertainty in surface mass balance-elevation
665 feedback on projections of the future sea level contribution of the Greenland ice sheet. *Cryosphere*, 8(1), 195-208.
666 2014.

667 Fowler, A.C. A sliding law for glaciers of constant viscosity in the presence of subglacial cavitation. In
668 *Proceedings of the Royal Society of London A: Mathematical, Physical and Engineering Sciences*, 407(1832),
669 147-170, 1986.

670 Fretwell, P., Pritchard, H.D., Vaughan, D., Bamber, J.L., Barrand, N.E., Bell, R., Bianchi, C., Bingham, R.G.,
671 Blankenship, D.D., Casassa, G. and Catania, G. Bedmap2: improved ice bed, surface and thickness datasets for
672 Antarctica. *Cryosphere*, 7, 375-393, 2013.

673 Fuchs, M. and Owen, L.A. Luminescence dating of glacial and associated sediments: review, recommendations
674 and future directions. *Boreas*, 37(4), 636-659, 2008.

675 Gasson, E., DeConto, R.M., Pollard, D. and Levy, R.H. Dynamic Antarctic ice sheet during the early to mid-
676 Miocene. *Proceedings of the National Academy of Sciences*, 113(13), 3459-3464, 2016.

677 Golledge, N.R., Levy, R.H., McKay, R.M., Fogwill, C.J., White, D.A., Graham, A.G., Smith, J.A., Hillenbrand,
678 C.D., Licht, K.J., Denton, G.H. and Ackert, R.P. Glaciology and geological signature of the Last Glacial
679 Maximum Antarctic ice sheet. *Quaternary Sci Rev*, 78, 225-247, 2013.

680 Gomez, N., Pollard, D., Mitrovica, J.X., Huybers, P., Clark, P.U. Evolution of a coupled marine ice sheet-sea
681 level model, *J Geophys Res*, 117, F01013, 2012.

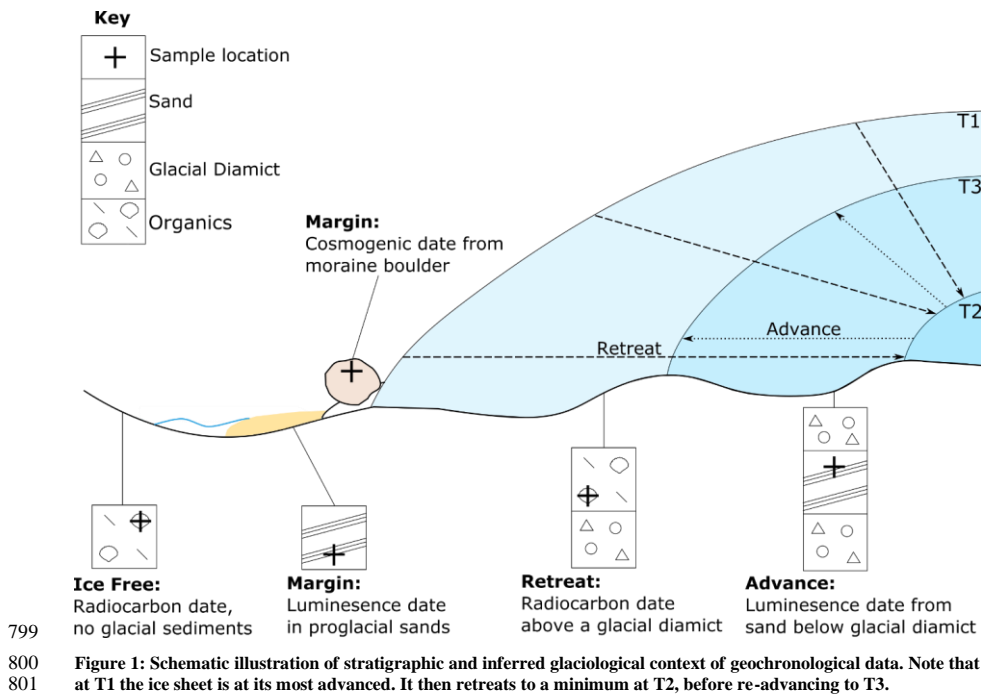
682 Gomez, N., Pollard, D. and Mitrovica, J.X. A 3-D coupled ice sheet-sea level model applied to Antarctica through
683 the last 40 ky. *Earth and Planet Sc Lett*, 384, 88-99, 2013.

684 Gowan, E.J. An assessment of the minimum timing of ice free conditions of the western Laurentide Ice Sheet.
685 *Quaternary Sci Rev*, 75, 100-113, 2013.

686 Gregoire, L.J., Payne, A.J. and Valdes, P.J. Deglacial rapid sea level rises caused by ice-sheet saddle collapses.
 687 *Nature*, 487(7406), 219-222, 2012.
 688 Greve, R. and Hutter, K. Polythermal three-dimensional modelling of the Greenland ice sheet with varied
 689 geothermal heat flux. *Ann Glaciol*, 21, 8-12, 1995.
 690 Gudmundsson, G.H., Krug, J., Durand, G., Favier, L. and Gagliardini, O. The stability of grounding lines on
 691 retrograde slopes. *Cryosphere*, 6, 1497-1505, 2012.
 692 Gudmundsson, G.H. Ice-shelf buttressing and the stability of marine ice sheets, *Cryosphere*, 7, 647-655, 2013.
 693 Heroy, D.C. and Anderson, J.B. Radiocarbon constraints on Antarctic Peninsula ice sheet retreat following the
 694 Last Glacial Maximum (LGM). *Quaternary Sci Rev*, 26(25), 3286-3297, 2007.
 695 Heyman, J., Stroeve, A.P., Harbor, J.M. and Caffee, M.W. Too young or too old: evaluating cosmogenic
 696 exposure dating based on an analysis of compiled boulder exposure ages. *Earth Planet Sc Lett*, 302(1), 71-80,
 697 2011.
 698 Hindmarsh, R.C. Consistent generation of ice-streams via thermo-viscous instabilities modulated by membrane
 699 stresses. *Geophys Res Lett*, 36(6). 2009.
 700 Hubbard, A., Bradwell, T., Gollledge, N., Hall, A., Patton, H., Sugden, D., Cooper, R. and Stoker, M. Dynamic
 701 cycles, ice streams and their impact on the extent, chronology and deglaciation of the British-Irish ice sheet.
 702 *Quaternary Sci Rev*, 28(7), 758-776, 2009.
 703 Hughes, A.L., Greenwood, S.L. and Clark, C.D. Dating constraints on the last British-Irish Ice Sheet: a map and
 704 database. *J Maps*, 7(1), 156-184, 2011.
 705 Hughes, A.L., Clark, C.D. and Jordan, C.J. Flow-pattern evolution of the last British Ice Sheet. *Quaternary Sci*
 706 *Rev*, 89, 148-168, 2014.
 707 Hughes, A.L., Gyllencreutz, R., Lohne, Ø.S., Mangerud, J. and Svendsen, J.I. The last Eurasian ice sheets –a
 708 chronological database and time-slice reconstruction, DATED-1. *Boreas*, 45(1), 1-45, 2016.
 709 Hughes, T.J., Is the West Antarctic ice sheet disintegrating? *J. Geophys. Res.*, 78 (33), 7884-7910, 1973.
 710 Imbrie, J., Hays, J.D., Martinson, D.G., McIntyre, A., Mix, A.C., Morley, J.J., Pisias, N.G., Prell, W.L.,
 711 Shackleton, N.J. The orbital theory of Pleistocene climate: support from a revised chronology of the marine $\delta^{18}\text{O}$
 712 record. In: Berger, A., Imbrie, J., Hays, H., Kukla, G., Saltzman, B. (Eds.), *Milankovitch and Climate, Part I*. D.
 713 Reidel Publishing, Dordrecht, 269–305, 1984.
 714 Johnsen, S.J., Dahl-Jensen, D., Dansgaard, W. and Gundestrup, N. Greenland palaeotemperatures derived from
 715 GRIP bore hole temperature and ice core isotope profiles. *Tellus B*, 47(5), 624-629, 1995.
 716 Kirchner, N., Hutter, K., Jakobsson, M. and Gyllencreutz, R. Capabilities and limitations of numerical ice sheet
 717 models: a discussion for Earth-scientists and modelers. *Quaternary Sci Rev*, 30(25), 3691-3704, 2011.
 718 Kirchner, N., Ahlkrone, J., Gowan, E.J., Lötstedt, P., Lea, J.M., Noormets, R., von Sydow, L., Dowdeswell, J.A.
 719 and Benham, T. Shallow ice approximation, second order shallow ice approximation, and full Stokes models: A
 720 discussion of their roles in palaeo-ice sheet modelling and development. *Quaternary Sci Rev*, 147, 136-147, 2016.
 721 Kleman, J., Hättestrand, C., Stroeve, A.P., Jansson, K.N., De Angelis, H. and Borgström, I. Reconstruction of
 722 Palaeo-Ice Sheets-Inversion of their Glacial Geomorphological Record. In Knight, P.G. (Eds) *Glacier science and*
 723 *environmental change*, 192-198, 2006.
 724 Larour, E., Seroussi, H., Morlighem, M. and Rignot, E. Continental scale, high order, high spatial resolution, ice
 725 sheet modeling using the Ice Sheet System Model (ISSM). *J Geophys Res-Earth*, 117(F1), 2012.

726 Libby, W.F., Anderson, E.C. and Arnold, J.R. Age determination by radiocarbon content: world-wide assay of
 727 natural radiocarbon. *Science*, 109(2827), 227-228, 1949.
 728 Lingle, C.S. and Clark, J.A. A numerical model of interactions between a marine ice sheet and the solid earth:
 729 Application to a West Antarctic ice stream. *J Geophys Res-Oceans*, 90(C1), 1100-1114, 1985.
 730 Livingstone, S.J., Cofaigh, C.Ó., Stokes, C.R., Hillenbrand, C.D., Vieli, A. and Jamieson, S.S. Antarctic palaeo-
 731 ice streams. *Earth-Sci Rev*, 111(1), 90-128, 2012.
 732 Lorenz, E.N. Deterministic Nonperiodic Flow, *J. Atmos. Sci.*, 20, 130-141, 1963.
 733 Lowe, J.J. and Walker, M.J. Radiocarbon Dating the Last Glacial-Interglacial Transition (Ca. 14–9 14C Ka Bp)
 734 in Terrestrial and Marine Records: The Need for New Quality Assurance Protocols. *Radiocarbon*, 42(1), 53-68,
 735 2000.
 736 Lowell, T.V., Fisher, T.G., Hajdas, I., Glover, K., Loope, H. and Henry, T. Radiocarbon deglaciation chronology
 737 of the Thunder Bay, Ontario area and implications for ice sheet retreat patterns. *Quaternary Sci Rev*, 28(17), 1597-
 738 1607, 2009.
 739 Lukas, S., Spencer, J.Q., Robinson, R.A. and Benn, D.I. Problems associated with luminescence dating of Late
 740 Quaternary glacial sediments in the NW Scottish Highlands. *Quaternary Geochron*, 2(1), 243-248, 2007.
 741 Mercer, J.H. West Antarctic ice sheet and CO2 greenhouse effect: a threat of disaster. *Nature*, 271, 321-325, 1978.
 742 Napieralski, J., Harbor, J. and Li, Y. Glacial geomorphology and geographic information systems. *Earth-Sci Rev*,
 743 85(1), 1-22, 2007.
 744 Ó Cofaigh, C.Ó. and Evans, D.J. Radiocarbon constraints on the age of the maximum advance of the British–Irish
 745 Ice Sheet in the Celtic Sea. *Quaternary Sci Rev*, 26(9), 1197-1203, 2007.
 746 Patton, H., Hubbard, A., Andreassen, K., Winsborrow, M. and Stroeven, A.P. The build-up, configuration, and
 747 dynamical sensitivity of the Eurasian ice-sheet complex to Late Weichselian climatic and oceanic forcing.
 748 *Quaternary Sci Rev*, 153, 97-121, 2016.
 749 Pattyn, F. Sea-level response to melting of Antarctic ice shelves on multi-centennial timescales with the fast
 750 Elementary Thermomechanical Ice Sheet model (f. ETISH v1. 0). *Cryosphere*, 11(4), p.1851-1878, 2017.
 751 Pattyn, F., Perichon, L., Aschwanden, A., Breuer, B., De Smedt, B., Gagliardini, O., Gudmundsson, G.H.,
 752 Hindmarsh, R., Hubbard, A., Johnson, J.V. and Kleiner, T. Benchmark experiments for higher-order and full
 753 Stokes ice sheet models (ISMIP-HOM). *Cryosphere*, 2(1), 111-151, 2008.
 754 Pattyn, F., Schoof, C., Perichon, L., Hindmarsh, R.C.A., Bueler, E., Fleurian, B.D., Durand, G., Gagliardini, O.,
 755 Gladstone, R., Goldberg, D. and Gudmundsson, G.H. Results of the marine ice sheet model intercomparison
 756 project, MISMIP. *Cryosphere*, 6(3), 573-588, 2012.
 757 Pollard, D. and DeConto, R.M. Modelling West Antarctic ice sheet growth and collapse through the past five
 758 million years. *Nature*, 458(7236), 329-332, 2009.
 759 Ritz, C., Edwards, T.L., Durand, G., Payne, A.J., Peyaud, V. and Hindmarsh, R.C. Potential sea-level rise from
 760 Antarctic ice-sheet instability constrained by observations. *Nature*, 528(7580), 115-118, 2015.
 761 Robinson, A., Calov, R. and Ganopolski, A. Greenland ice sheet model parameters constrained using simulations
 762 of the Eemian Interglacial. *Clim Past*, 7(2), 381-396, 2011.
 763 Rutt, I.C., Hagdorn, M., Hulton, N.R.J. and Payne, A.J. The Glimmer community ice sheet model. *J Geophys*
 764 *Res-Earth*, 114(F2), 2009.

765 Schoof, C.S. Ice sheet grounding line dynamics: steady states, stability and hysteresis. *J. Geophys. Res. Earth*
 766 *Surf.*, 112, F03S28, 2007.
 767 Schoof, C. Coulomb friction and other sliding laws in a higher-order glacier flow model. *Math Mod Meth Appl*
 768 *S*, 20(01), 157-189, 2010.
 769 Schoof, C. Marine ice sheet stability. *J. Fluid Mech.*, 698, 62-72, 2012.
 770 Seddik, H., Greve, R., Zwinger, T., Gillet-Chaulet, F. and Gagliardini, O. Simulations of the Greenland ice sheet
 771 100 years into the future with the full Stokes model Elmer/Ice. *J Glaciol*, 58(209), 427-440, 2012.
 772 Seguinot, J., Rogozhina, I., Stroeve, A.P., Margold, M. and Kleman, J. Numerical simulations of the Cordilleran
 773 ice sheet through the last glacial cycle. *Cryosphere*, 10, 639-664, 2016.
 774 Simpson, M.J., Milne, G.A., Huybrechts, P. and Long, A.J. Calibrating a glaciological model of the Greenland
 775 ice sheet from the Last Glacial Maximum to present-day using field observations of relative sea level and ice
 776 extent. *Quaternary Sci Rev*, 28(17), 1631-1657, 2009.
 777 Small, D., Clark, C.D., Chiverrell, R.C., Smedley, R.K., Bateman, M.D., Duller, G.A., Ely, J.C., Fabel, D.,
 778 Medialdea, A. and Moreton, S.G. Devising quality assurance procedures for assessment of legacy
 779 geochronological data relating to deglaciation of the last British-Irish Ice Sheet. *Earth-Sci Rev*, 164, 232-250,
 780 2017.
 781 Smedley, R.K., Glasser, N.F. and Duller, G.A.T. Luminescence dating of glacial advances at Lago Buenos Aires
 782 ($\sim 46^\circ$ S), Patagonia. *Quaternary Sci Rev*, 134, 59-73, 2016.
 783 Smedley, R.K., Chiverrell, R.C., Ballantyne, C.K., Burke, M.J., Clark, C.D., Duller, G.A.T., Fabel, D., McCarroll,
 784 D., Scourse, J.D., Small, D. and Thomas, G.S.P. Internal dynamics condition centennial-scale oscillations in
 785 marine-based ice-stream retreat. *Geology*, 45(9), 787-790, 2017.
 786 Stokes, C.R., Tarasov, L., Blomdin, R., Cronin, T.M., Fisher, T.G., Gyllencreutz, R., Hättestrand, C., Heyman, J.,
 787 Hindmarsh, R.C., Hughes, A.L. and Jakobsson, M. On the reconstruction of palaeo-ice sheets: recent advances
 788 and future challenges. *Quaternary Sci Rev*, 125, 15-49, 2015.
 789 Tarasov, L. and Peltier, W.R. A geophysically constrained large ensemble analysis of the deglacial history of the
 790 North American ice-sheet complex. *Quaternary Sci Rev*, 23(3), 359-388, 2004.
 791 Tarasov, L., Dyke, A.S., Neal, R.M. and Peltier, W.R. A data-calibrated distribution of deglacial chronologies for
 792 the North American ice complex from glaciological modeling. *Earth Planet Sc Lett*, 315, 30-40, 2012.
 793 Tushingham, A.M. and Peltier, W.R. Validation of the ICE-3G Model of Würm-Wisconsin Deglaciation using a
 794 global data base of relative sea level histories. *J Geophys Res-Solid Earth*, 97(B3), 3285-3304, 1992.
 795 Weertman, J. Stability of the junction of an ice-sheet and an ice-shelf. *J. Glaciol*. 13 (67), 3-11, 1974.
 796 Winkelmann, R., Martin, M.A., Haseloff, M., Albrecht, T., Bueller, E., Khroulev, C. and Levermann, A. The
 797 Potsdam parallel ice sheet model (PISM-PIK)-Part 1: Model description. *Cryosphere*, 5(3), 715-726, 2011.
 798



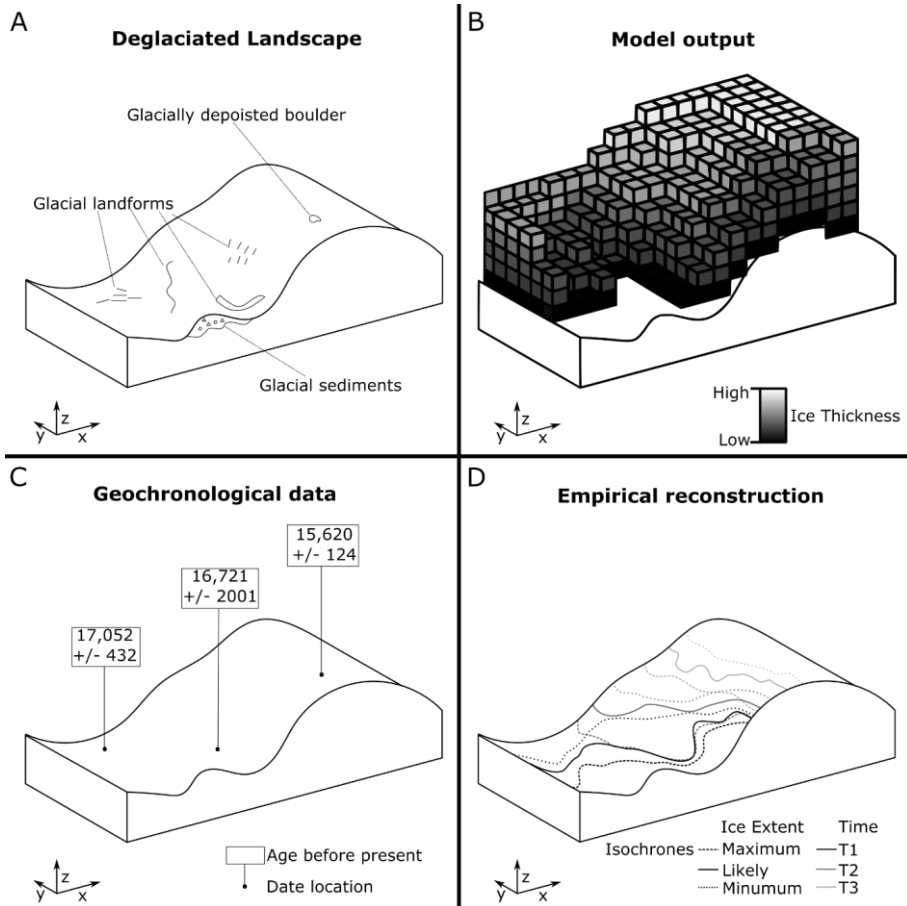


Figure 2. Schematic of geochronological data and ice-sheet model output. A) A deglaciated landscape, demonstrating some of the features used by palaeo-glaciologists when empirically reconstructing an ice sheet. B) Ice-sheet model output, displaying modelled ice-sheet thickness, in this case at a specific time. C) Geochronological data. D) Empirical reconstruction. Note how the nature of these data vary between source.

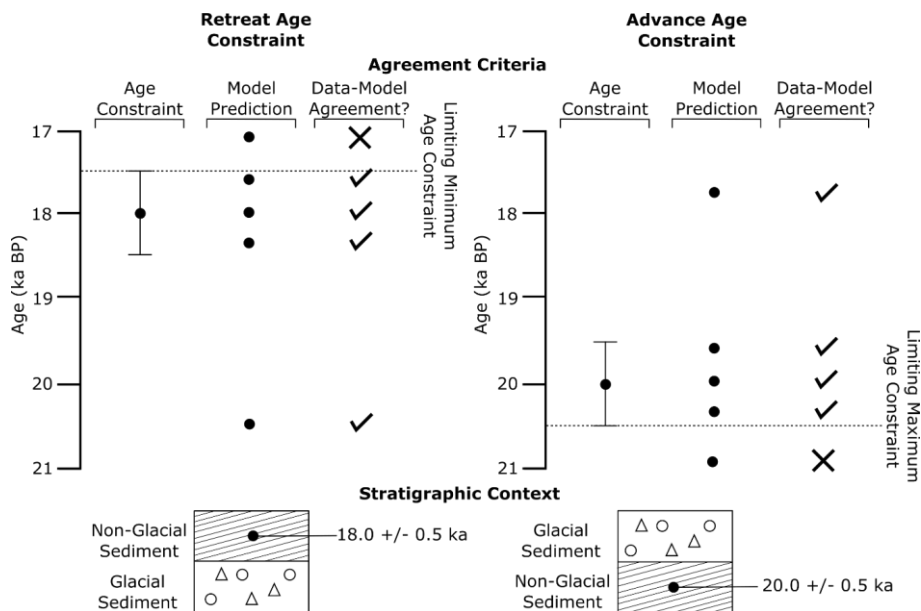


Figure 3. Identification of data-model agreement with consideration of error by ATAT for retreat (left) and advance (right) data. If a model predicts ice free conditions before an ice-free age, or during the associated error, there is data-model agreement. If deglaciation occurs at this location after the error, the model disagrees with the data. If a model predicts ice advance and cover before the advance age and its associated error, there is model-data disagreement. Agreement between the model and data occurs if ice advances over the location after the date, or before the date within the range of the error.

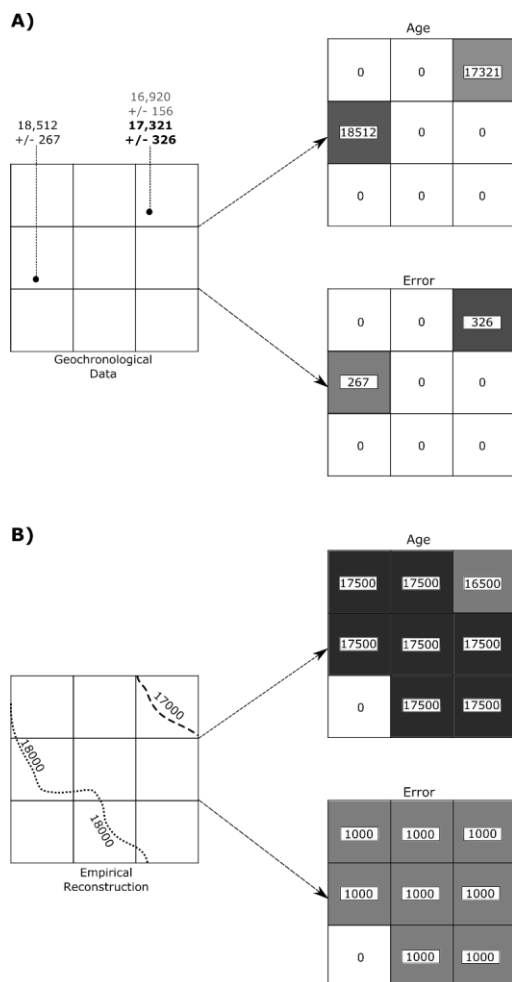
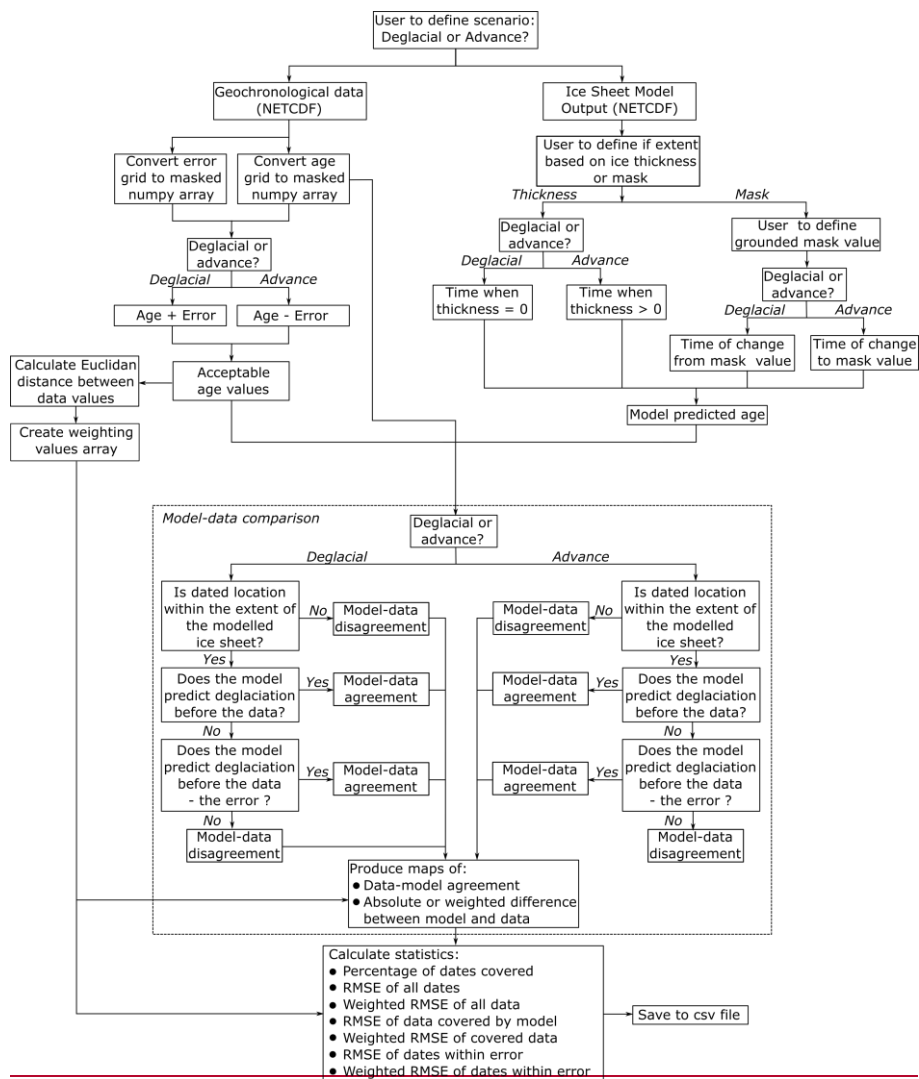


Figure 4. Examples of empirical data preparation for ATAT. (A) Conversion of geochronological data into a grid for ATAT. In this example the user has made a judgement based on a priori knowledge that the date of $17,321 \pm 326$ is most representative of the event of interest. Note that age and error are split into separate grids, and that no data regions are assigned a value of 0. (B) Conversion of an empirical reconstruction (margin isochrones) into a grid for ATAT. Here we simply assume that the area between isochrones became deglaciated between at the age between the two isochrones, and that associated error is 1000 years. More complex reconstructions (e.g. Hughes et al., 2016) may require different user-defined rules.



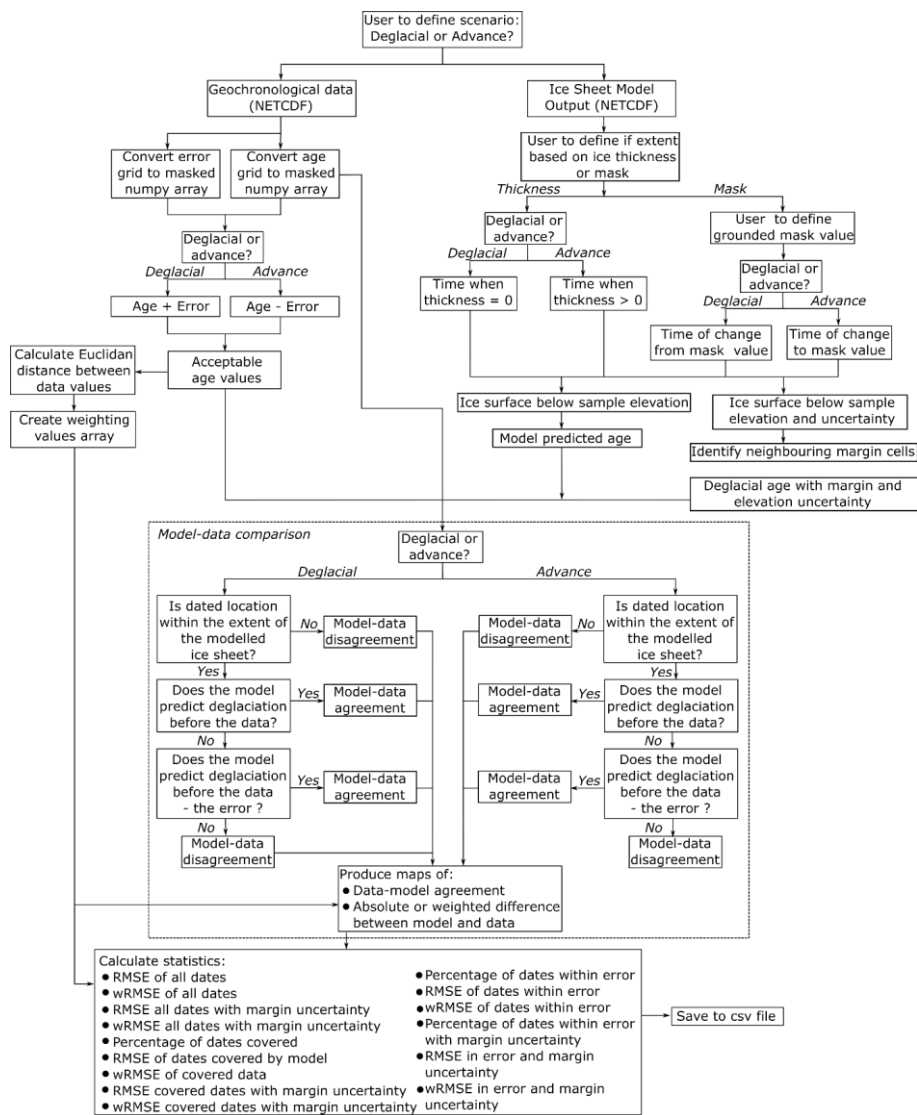


Figure 5. Flow chart of ATAT procedure. See text for further description.

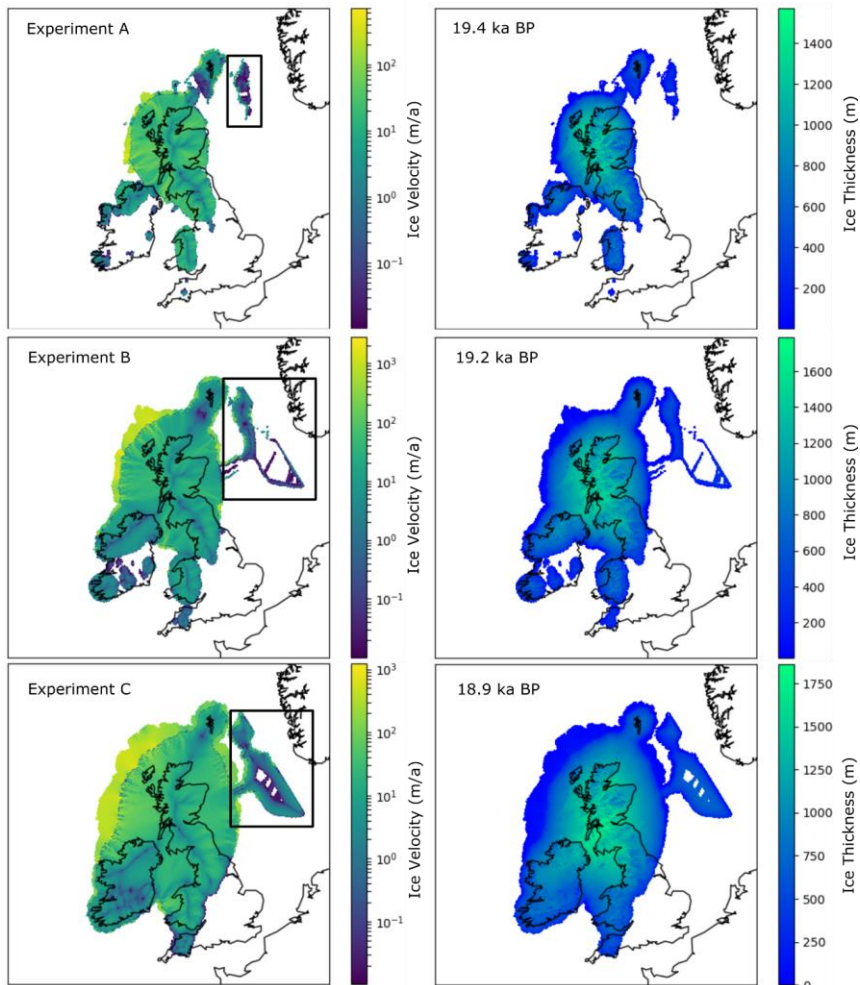
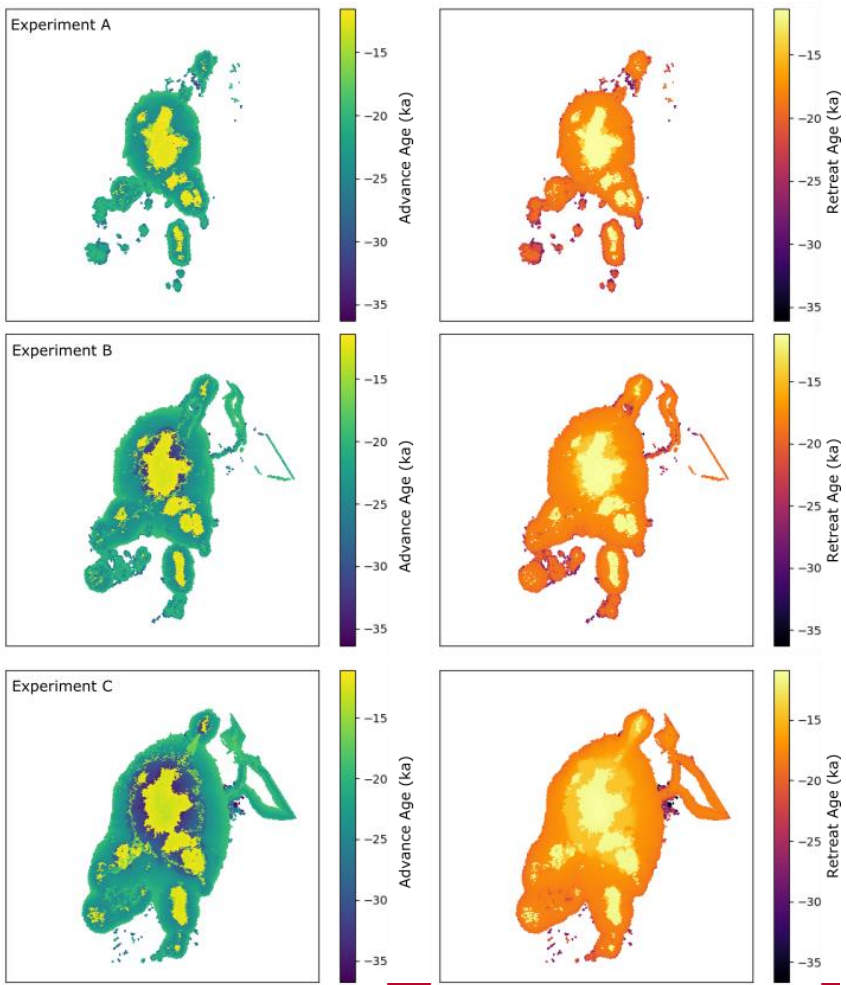


Figure 6. Maximum extent of produced ice sheet for the three experiments. Experiment B is 1°C colder than A, and experiment C is 2°C colder than A. Left panel shows ice velocity, right is ice thickness. The box on the left panel highlights likely erroneous output in the North Sea, likely a consequence of model domain, discussed further in the text.



831

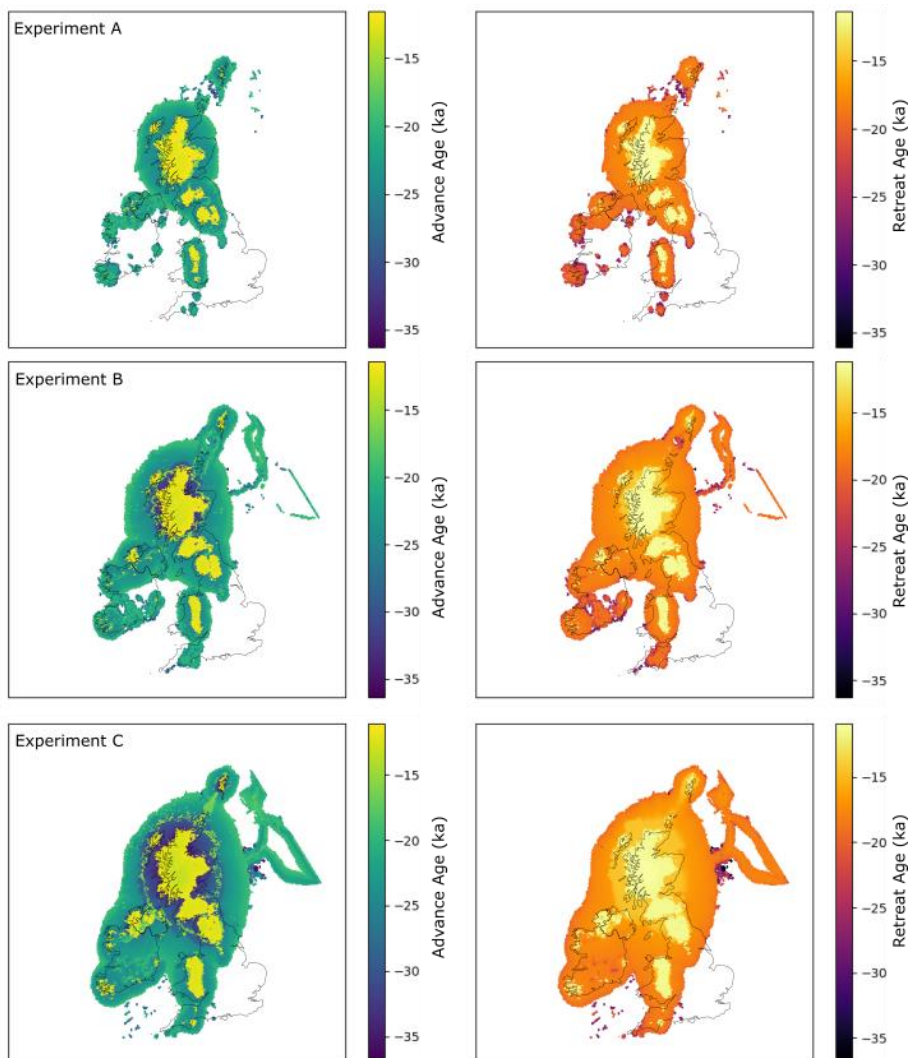
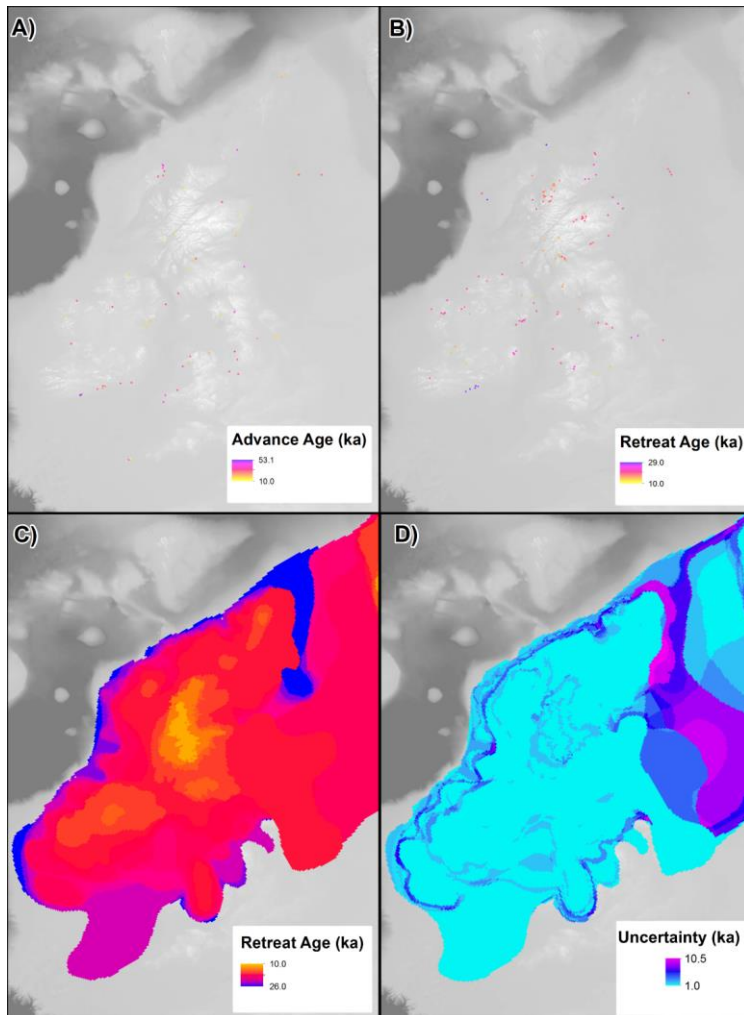


Figure 7. Timing of advance (left) and retreat (right) from the three ice sheet modelling experiments. Experiments are the same as in Figure 6. The early ages toward the centre of the model, and centred over higher topography, represent the modelled extent of the Younger Dryas readvance.



836

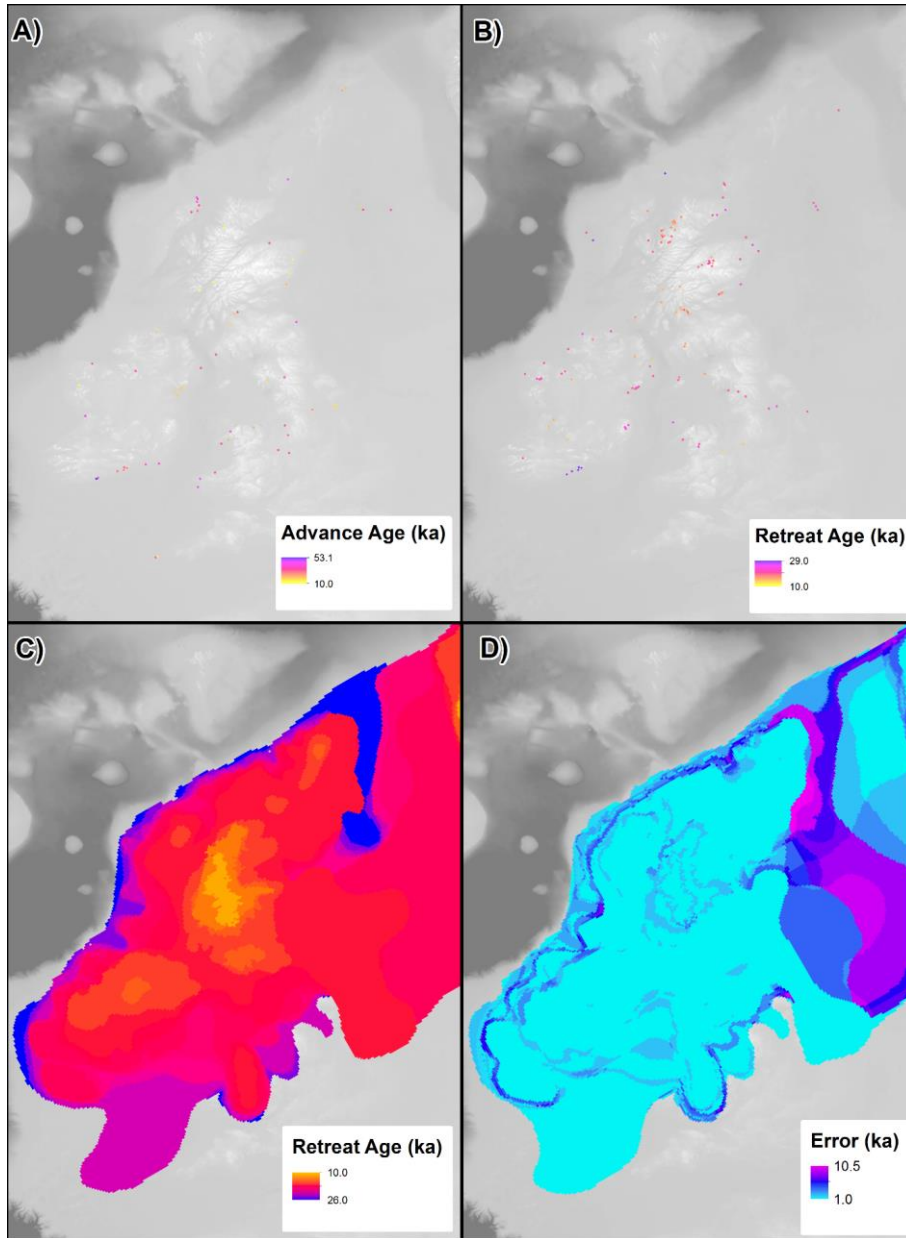


Figure 8. Example of geochronological data projected onto model raster grids; as point-data in A and B and from an empirical reconstruction in C and D. (A). Advance ages from Hughes et al. (2016). (B) Retreat ages from Small et al. (2017). (C) Retreat age derived from DATED isochrone reconstruction (Hughes et al., 2016). (D) Error associated with reconstruction in C.

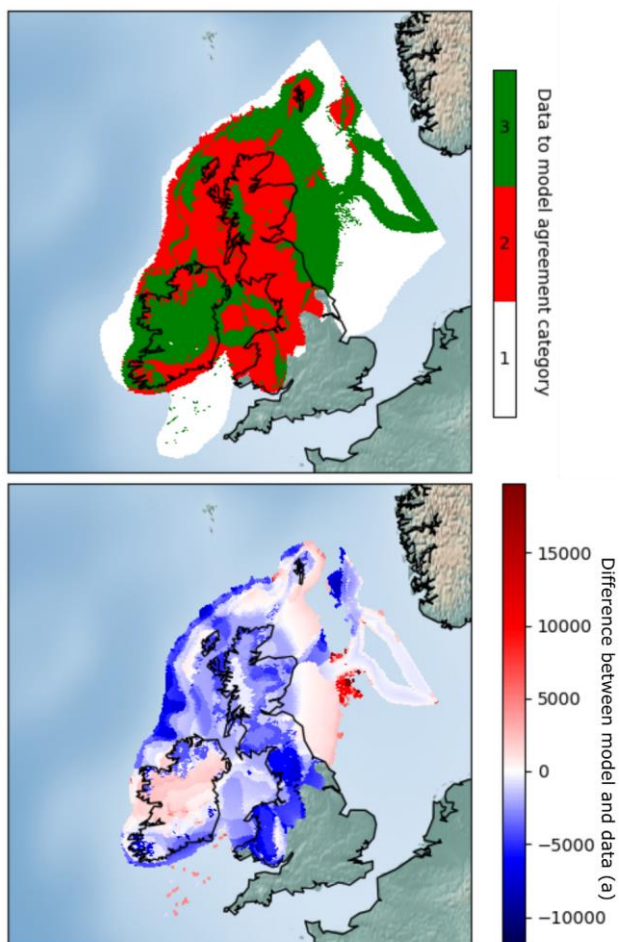


Figure 9. Example mapped outputs from ATAT. In this case, experiment C was compared with the DATED reconstruction. Top map (cumulative agreement) shows categories of data-model agreement across the domain, where 1 = not covered by model, 2 = no agreement and 3 = data-model agreement within error. The lower map (model-data offset) shows magnitude of difference between model and data; negative values show a modelled retreat of ice later than the DATED isochrones, and positive values show a modelled retreat of ice before the DATED isochrones.

849 Table 1. Classification of geochronological data (after Hughes et al., 2011) and its use in ATAT.

Class	Glaciological context	Stratigraphic context	Example	Use in ATAT
Advance	Ice-sheet build up	Material directly below or incorporated within glacial diamict	Luminescence date from a sand below a glacial diamict	Ice cover a short time after this date
Retreat	Ice-free after ice cover	Dated material above glacial diamict	Radiocarbon date of a shell above a glacial diamict	Ice-free conditions from this date onwards (note deglaciation could have occurred a long time before)
Ice Free	Ice-free, but lacking direct information regarding ice	Dated material which indicates ice-free conditions but has no relation to ice cover. It may be much younger and not provide much useful constraint.	Radiocarbon date of organic sediments without underlying glacial sediments	
Margin	Proximal to an ice sheet margin	Dated material with information that ties it to an ice margin	Luminescence date in proglacial sands	
Exposure time (cumulative)	Length of time since sample exposed	N/A	Cosmogenic isotope on erratic boulder above a trimline	Not used

850

Table 2. Comparison of attributes between geochronological data and ice sheet model output.

	Nature of data produced	Spatial resolution	Spatial continuity	Temporal frequency and resolution	Sources of uncertainty	Main limitation
Geochronological data	Timing of the absence of ice at a location	Point location	Point location, unevenly distributed in space, but can be interpolated	Determined by data availability and associated error	Instrumental, environmental and stratigraphic factors	Reliant upon correct stratigraphic interpretation to tie to glaciological events
Ice-sheet model output	Simulation of physically plausible ice sheet conditions	Various, ranging from tens to unit kilometres.	Spatially even, regularly-spaced across entire domain	Continuous in time. Precise subannual resolution possible, but not recorded in practice	Parameterisations, boundary conditions	Based upon mathematical and physical approximations of ice flow

Data source	NetCDF Variable	Units	Dimensions	Description	Notes
Ice sheet model output	Time	Years before <u>Time</u> <u>unit</u> before <u>reference</u> <u>calendar</u> <u>date</u>	x, y	Calendar years before present	
	thk	m	time, x,y	Ice thickness	Either “thk” or “msk” required by ATAT.
	msk	Integers	time, x,y	Grounded/floating/icefree mask	Either “thk” or “msk” required by ATAT. User defines value referring to the location of grounded ice
	lat	Decimal degrees	x, y	Latitude	
	Both lon	Decimal degrees	x, y	Longitude	
Geochronological data	age	<u>Time</u> <u>unit</u> <u>before</u> <u>reference</u> <u>calendar</u> <u>date</u> Years before <u>present</u>	x, y	Timing of deglaciaded conditions	Deglacial and advance ages must be in separate files.
	error	Years <u>Secon</u> <u>ds</u>	x, y	Error associated with deglaciaded conditions	Error associated with either deglacial and advance age

must be in associated separate
file.

<u>topg</u>	<u>m</u>	<u>x,y</u>	<u>Modern elevation at resolution</u>
			<u>of ice-sheet model</u>
<u>elevation</u>	<u>m</u>	<u>x,y</u>	<u>Elevation of collected sample</u>

Table 3. Required input variables for ATAT NetCDF files.

Table 4: Example statistics from ATAT. Note that the RMSE is often altered by applying the spatial weighting to create wRMSE.

	<u>Advance</u>			<u>Retreat</u>			<u>Empirical Reconstruction:</u> <u>DATED</u>		
<u>Ice Sheet</u> <u>Modelling</u> <u>Experiment</u>	<u>A</u>	<u>B</u>	<u>C</u>	<u>A</u>	<u>B</u>	<u>C</u>	<u>A</u>	<u>B</u>	<u>C</u>
<u>Percentage</u> <u>of dates</u> <u>covered</u>	<u>52.5</u>	<u>72.1</u>	<u>88.5</u>	<u>76.1</u>	<u>91.7</u>	<u>96.3</u>	<u>32.9</u>	<u>52.6</u>	<u>69.8</u>
<u>Percentage</u> <u>that agree</u> <u>within error</u>	<u>65.6</u>	<u>72.7</u>	<u>72.2</u>	<u>22.0</u>	<u>22.0</u>	<u>12.8</u>	<u>23.2</u>	<u>27.0</u>	<u>17.8</u>
<u>RMSE</u> <u>dates</u> <u>covered by</u> <u>model</u>	<u>11075.9</u>	<u>12732.7</u>	<u>13490.3</u>	<u>3879.0</u>	<u>4180.9</u>	<u>4945.4</u>	<u>2972.5</u>	<u>2678.0</u>	<u>2920.8</u>
<u>wRMSE</u> <u>dates</u> <u>covered by</u> <u>model</u>	<u>13357.3</u>	<u>13994.7</u>	<u>14849.7</u>	<u>4073.4</u>	<u>4450.3</u>	<u>5165.8</u>	<u>N/A</u>	<u>N/A</u>	<u>N/A</u>
<u>RMSE</u> <u>dates within</u> <u>error</u>	<u>655.7</u>	<u>478.6</u>	<u>289.3</u>	<u>403.6</u>	<u>259.7</u>	<u>236.2</u>	<u>12023.4</u>	<u>10638.7</u>	<u>8777.6</u>

<u>wRMSE</u> <u>dates within</u> <u>error</u>	<u>615.4</u>	<u>395.0</u>	<u>223.6</u>	<u>422.1</u>	<u>276.9</u>	<u>248.9</u>	<u>N/A</u>	<u>N/A</u>	<u>N/A</u>
---	--------------	--------------	--------------	--------------	--------------	--------------	------------	------------	------------